

A New Method to Synthesize an SRS Compatible Base Acceleration with Energy and Temporal Moments to Improve MDOF System Response (First Part)

J. Edward Alexander

A new method has been developed to synthesize a shock response spectrum (SRS) compatible base acceleration with additional parameters in the synthesis process beyond current practices. Current base acceleration synthesis methods address only SRS compatibility. However, additional information is available to synthesize a base acceleration to improve multi-degree of freedom (MDOF) system response accuracy. Expanding the synthesis procedure to include energy input and temporal information provides more constraints on the development of the synthesized acceleration. Similar to the SRS, an energy input spectrum (EIS) is a frequency based relationship for the peak energy input per unit mass to a series of single-degree of freedom (SDOF) oscillators from a base acceleration. The EIS represents total input energy contributions (kinetic, damped and absorbed energy). Temporal information includes overall shape of the transient shock pulse envelope $E(t)$ (rise, plateau, decay) and five temporal moments. When EIS, $E(t)$ and temporal moments compatibility are added to the synthesis procedure, an improved base acceleration results. To quantify the significance of these quantities, a regression analysis was performed based on linear and nonlinear 3DOF model responses. The regression analysis confirmed that compatibility with SRS, EIS and temporal moments were significant factors to improve MDOF model response accuracy. To test this finding, a base acceleration was synthesized with the expanded procedure. Four other accelerations were synthesized with current state of the art methods which match the SRS only. The five synthesized accelerations were applied to a 3DOF model based on a US naval medium weight shock machine (MWSM). MWSM model results confirmed that the SRS, EIS, and temporal moment compatible acceleration resulted in improved accuracy of peak mass accelerations and displacements in the majority of the cases, and consistently gave more accurate peak energy input to the MWSM model. Energy input to a structure is a significant factor for damage potential. The total kinetic, damped and absorbed energy input represents a system damage potential which the structure as a whole must dissipate.

Nomenclature

3DOF Three degree of freedom
 a_D Design acceleration
 a_S Synthesized acceleration
 $asyn_{427k}$ Acceleration synthesized from merit function Eq. (3-16)-427k iterations
 A_n Amplitude of n^{th} sinusoid
 D Duration
 $D\%$ Duration percent error of a_S relative to a_D
 EI Energy input
 EIS Energy input spectrum
 EIS_D Energy input spectrum for a_D
 EIS_S Energy input spectrum for a_S
 $EIS_{asyn_{427k}}$ Energy input spectrum for $asyn_{427k}$
 $EIS\%$ EIS percent error of a_S relative to a_D averaged over frequency bandwidth
 En Total peak energy input to MDOF model
 EOM Equation of motion
 $E(t)$ Envelope function for synthesized acceleration
 f Frequency, Hz
 f_n Natural frequency of n^{th} SDOF oscillator, Hz
 g Acceleration due to gravity
 H_0 Null hypothesis in regression analysis
 H_1 Alternative hypothesis in regression analysis
 H_V Velocity transfer function
 Hz Hertz (cycles/second)
 i Iteration index for a_S synthesis iteration process
 $ITOP$ International test operations procedure
 j Index for j^{th} m , c and k in MDOF model
 k Index for time step increment
 k_j j^{th} spring stiffness in MDOF model
 K Kurtosis

$K\%$ Kurtosis percent error of a_S relative to a_D
 KPH Kilometers per hour
 M Merit function
 m Mass
 m_i i^{th} temporal moment
 m_j j^{th} mass in MDOF model
 $MDOF$ Multi-degree of freedom
 MOD Ministry of Defense
 $MWSM$ Medium weight shock machine
 N_n Number of half sines in n^{th} wavelet
 n Frequency index
 P_n Participation factor for n^{th} mode of vibration
 PSD Power spectral density
 R^2 Percent that regression model explains the variation in response
 REA Root energy amplitude
 RMS Root mean squared
 S Skewness
 $S\%$ Percent skewness error of a_S relative to a_D
 $SDOF$ Single degree of freedom
 SRS Shock response spectrum
 SRS_D Shock response spectrum for a_D
 SRS_S Shock response spectrum for a_S
 $SRS_{asyn_{427k}}$ Shock response spectrum for $asyn_{427k}$
 SRS_{vel} Velocity SRS
 $SRS\%$ SRS percent error of a_S relative to a_D averaged over frequency bandwidth
 t_{dn} Wavelet time delay
 $u(t)$ Absolute acceleration
 $\dot{u}(t)$ Absolute velocity
 $\ddot{u}(t)$ Absolute acceleration
 $\ddot{u}_b(t)$ Base acceleration
 UK United Kingdom
 W_{EIS} EIS% weighting in merit function (M) equation
 W_{SRS} SRS% weighting in merit function (M) equation
 x Modal coordinate
 $\dot{x}(t)$ Modal coordinate velocity
 $\ddot{x}(t)$ Modal coordinate acceleration
 $z(t)$ Relative displacement
 $\dot{z}(t)$ Relative velocity
 $\ddot{z}(t)$ Relative acceleration

Greek Alphabet Nomenclature:

α Mass matrix coefficient for Raleigh damping
 β Stiffness matrix coefficient for Raleigh damping
 Δ Elastic limit for nonlinear-elastic springs in 3DOF models
 ζ Percent of critical damping
 ϕ_n Phase angle for n^{th} sinusoid
 ω_i Circular frequency for i^{th} mode of vibration, radians/second
 ω_n Natural frequency of n^{th} SDOF oscillator, radians/second
 τ Temporal centroid of a wave form
 $\tau\%$ percent error of centroid location of a_S relative to a_D
 ϵ Discrete point in time

Matrix Nomenclature:

[C] Damping matrix
 $[C_L]$ Linear part of damping matrix
 $[C_{NL}]$ Nonlinear part of damping matrix which is function of velocity
 $[K]$ Stiffness matrix
 $[K_L]$ Linear part of stiffness matrix
 $[K_{NL}]$ Nonlinear part of stiffness matrix which is function of displacement
 $[M]$ Mass matrix
 $\{x_i\}$ Modal coordinate vector for mode i
 $\{u\}$ Absolute displacement vector
 $\{z\}$ Relative displacement vector
 $\{\ddot{z}\}$ Relative acceleration vector
 $\{\phi\}_n$ Mode shape vector for mode n
 $[\Phi]$ Mode transformation matrix

1 Spectral Methods to Characterize Shock and Energy

1.1 Overview

The shock response spectrum (*SRS*), conceived by Maurice Biot (1932), has been used as a structural dynamic method to characterize the seismic and mechanical shock environment for more than eight decades. The *SRS*, by definition, is the peak acceleration response of a series of single-degree-of-freedom (*SDOF*) mechanical oscillators of different frequencies, all with same the percent of critical damping, subjected to the same transient base input acceleration. The *SRS* is most frequently presented as a log-log graph of the peak *SDOF* acceleration responses as a function of the frequency bandwidth of interest. Early research and application of the *SRS* was conducted in the 1950's by the seismic community^{29, 35} to characterize the earthquake seismic shock environment. After the 1950's the use of the *SRS* expanded significantly for the seismic, aerospace and defense communities. The *SRS* is frequently employed to specify the design requirement for the structural dynamic shock environment that a physical system must survive^{10, 15, 45, 46}.

When structural dynamic requirements are specified in terms of a design shock response spectrum, termed *SRS_D*, the evaluation of a structure to meet this requirement can be demonstrated by either analysis or test. If it can be demonstrated the structure will survive the input shock specified by *SRS_D* and continue to meet operational requirements, it is considered to be shock qualified. When the system to be shock qualified can be modelled as a linear structure (i.e. linear equations of motion), a mode superposition analysis procedure can be performed directly, using *SRS_D*, to estimate the peak dynamic response (accelerations, displacements) of a multi-degree of freedom (*MDOF*) system.

However, if the structure is to be shock qualified by electro-dynamic shaker testing, or if the structure to be analyzed is nonlinear (i.e. nonlinear equations of motion), the *SRS_D* cannot be used directly. In these instances an *SRS_D* compatible acceleration time-history, *a_S*, must be synthesized. The synthesized *a_S* can be input directly as a transient base acceleration for transient analysis of the nonlinear *MDOF* model, or to drive the armature of an electro-dynamic shock test machine.

Synthesis of an *SRS_D* compatible base acceleration time-history is not difficult to execute and numerous procedures have been documented for this purpose. However, past research has demonstrated that synthesis of an *SRS_D* compatible acceleration time-history *a_S* does not, by itself, guarantee that the peak dynamic structure responses will be accurate. Accurate, in the context of this document, is defined as system response from a synthesized base acceleration that matches the corresponding system response from a design acceleration with good accuracy, for example within 10%. Current *SRS_D* compatible synthesis methods do not consider compatibility with the energy input spectrum (*EIS*) nor the temporal characteristics of *a_S*. Motivation for the research documented herein is to augment existing *SRS_D* compatible transient acceleration *a_S* synthesis processes to improve the accuracy of peak *MDOF* system response. Additional constraints beyond only *SRS_D* compatibility are:

- Matching the energy input to the structure based on the synthesized acceleration's compatibility with the energy input spectrum (*EIS*) and,
- Constraining the synthesized acceleration to match predefined temporal characteristics, termed temporal moments

1.2 Shock Response Spectrum Definition

Shock is a major structural design consideration for a wide variety of systems and their components. Shock is a sudden, sometimes violent, change in velocity (rapid acceleration) of a physical system due to the transient application of an external force or acceleration. The shock response spectrum is a way to characterize the frequency response of a series of single degree-of-freedom (*SDOF*) systems all subjected to the same transient base input shock acceleration. The *SRS* has been used for more than 80 years to characterize the frequency response from transient shock acceleration. The *SRS* is defined simply as the peak acceleration response (either positive or negative) of a series of base excited linear *SDOF* oscillators of different frequencies subjected to the same transient base acceleration input.

Figure (1-1) is a graphical representation of how an *SRS* is determined. Consider a base transient shock input acceleration time-history where the entire base experiences this acceleration. A series of *SDOF* linear oscillators of different frequencies mounted on the rigid base will also experience this transient shock acceleration input. To illustrate the *SRS*, the response of six *SDOF* oscillators is examined in this example. These *SDOF* oscillators are

tuned to frequencies of 30 Hz, 60 Hz, 200 Hz, 500 Hz, 1000Hz and 1300 Hz. The transient mass acceleration response of each is plotted above the corresponding *SDOF* oscillator and the peak value is indicated on each plot. For example, the peak acceleration response of the 30 Hz *SDOF* oscillator is -10.46 g as indicated on the plot, which is the lowest magnitude of the six *SDOF* oscillators. The peak amplitude of the 60 Hz *SDOF* oscillator is 22.7 g. The *SDOF* peak amplitudes continue to increase to 151.2 g for the 1300 Hz oscillator. Had higher frequency oscillators been included in this example, at some *SDOF* frequency, the peak *SDOF* acceleration response value would reach a maximum. For *SDOF* oscillators with frequencies above this limiting frequency, the peak acceleration response would begin to decrease. In the limit, at the extreme high frequency end of the spectrum, the peak amplitude of the highest frequency oscillator would asymptotically converge to 47.5 g, which is the peak amplitude of the input base acceleration. This is because, at the high frequency end of the spectrum, the *SDOF* oscillator is so stiff that it acts like a rigid (infinitely stiff) element attached to the base, and as such experiences acceleration identical to that of the base input acceleration. The *SRS* approaching the high frequency asymptote is demonstrated by the *SRS* of Figure (2-3) in Chapter 2.

The peak acceleration response of each of the six *SDOF* oscillators is plotted as a function of frequency at the top of Figure (1-1). These six points are indicated on the *SRS* plot at the corresponding frequencies of each oscillator. It is noted that the peak acceleration of each *SDOF* oscillator do not occur at the same point in time during the transient. The *SRS* gives the peak response of each *SDOF*, but does not retain temporal information as to when the peak occurs. The complete *SRS* is developed for *SDOF* oscillators covering the frequency band width of interest, 10 Hz to 3000 Hz in this case. A good overview of the early historical development of the *SRS* is given by Trifunac (2008)

1.3 Shock Response Spectrum *SRS_D* as a Shock Design Specification

The *SRS* is used widely in the defense, aerospace and seismic communities. The *SRS* is often prescribed as a structural design shock design specification, termed *SRS_D* herein, to characterize the requirement for the structural shock design environment. A design shock response spectrum *SRS_D* is frequently determined from platform (i.e. ship, ground vehicle, etc.) field testing. In these cases, numerous transient accelerations data records are taken during testing. Figure (1-2) is an illustrative example of multiple acceleration-time histories from field tests. The test acceleration signals also provide typical shock pulse temporal parameters (rise time, decay time, strong shock duration, overall shock pulse envelope) for a particular shock event (underwater explosions, earthquakes, pyrotechnics, ballistic impact, etc.). The acceleration-time histories from platform field tests can be transformed to an ensemble of shock response spectra as illustrated in Figure (1-2). The transformation to an *SRS* gives the *SDOF* response maxima for all frequencies. However, as demonstrated by the transient plots of Figure (1-1), the peak mass accelerations do not occur at the same time. As such, the *SRS* does not retain the timing of when the transient acceleration peaks occurs. In order to develop a single design *SRS_D*, a maximum envelope of all spectra is constructed. A single design *SRS_D* which envelopes all *SRS*; is illustrated by the graph on the right side of the Figure (1-2).

There are numerous examples where structural dynamic environment requirements for a shock event are specified by a design *SRS_D*. The seismic environment for ground structures was the first case of this approach for design. Housner²⁷ published both velocity and acceleration spectra based on enveloping the four strongest earthquake ground motions recorded at the time (El Centro-1934, El Centro-1940, Olympia-1949, Tehachapi-1952). Subsequently, Newmark, et al.⁴⁹ published a recommended design shock response spectrum *SRS_D* for nuclear power plants based on the evaluation of seventeen recorded earthquake horizontal and vertical accelerations.

The Newmark horizontal design *SRS_D*, Figure (1-3), has survived for more than 40 years and remains the U. S. Nuclear Regulatory Commission's *SRS_D* requirement for nuclear power plants as specified in Regulatory Guide 1.60⁶⁷.

Similar shock response spectrum requirements for equipment aboard US naval ships were first published by the Naval Research Laboratory in 1963. In the case of shipboard equipment, the design spectra is specified based on the type of ship (surface ship or submarine) and the mounting location of the equipment in the ship, (hull, deck or shell mounted). Interim unclassified design *SRS_D* values were first published by Naval Research Lab Engineers O' Hara and Belsheim⁵⁰.

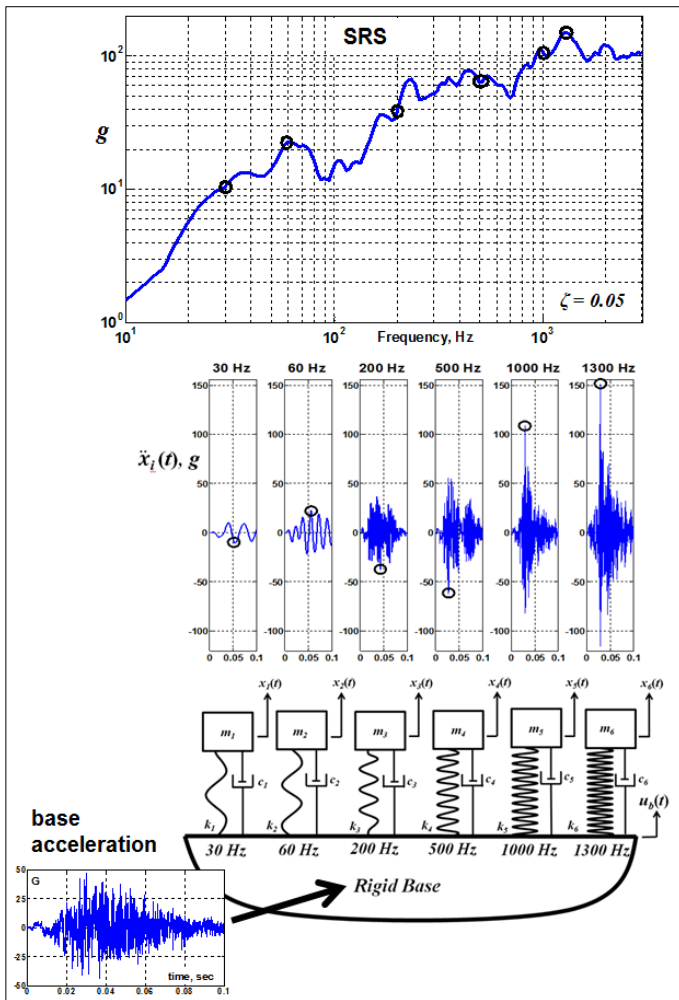


Figure (1-1). Graphical Representation of the Shock Response Spectrum.

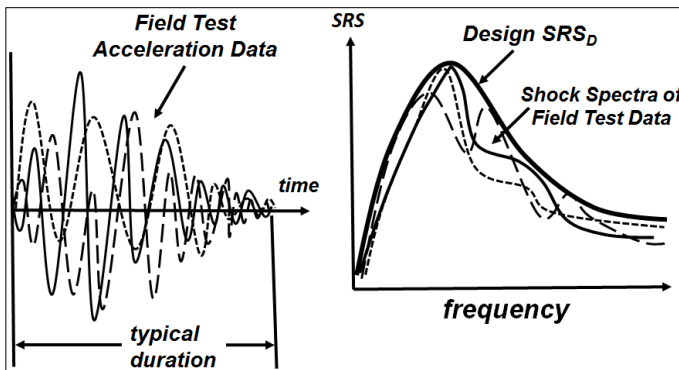


Figure (1-2). Development of a Design SRSD from Field Test Data.

Subsequently a classified SRS_D requirements document was issued by the US Navy¹⁶. This document remains the US Navy's SRS_D requirement for shock qualification of naval equipment by analysis.

For other military equipment, MIL-STD-810G, Method 516, Shock⁴² specifies requirements for a several shock qualification SRS_D . If field test data are available, the general 810 G guidance is to determine SRS_D with the maximum envelope approach illustrated in Figure (1-2). Further, it is possible to determine a temporal duration T_E , defined in Section 3.2, if recorded time history test data are available from field testing. If measured test data are not available, the guidance for functional and crash hazard shock is to use prescribed SRS_D published in MIL-STD-810G, Method 516, Figure (1-4).

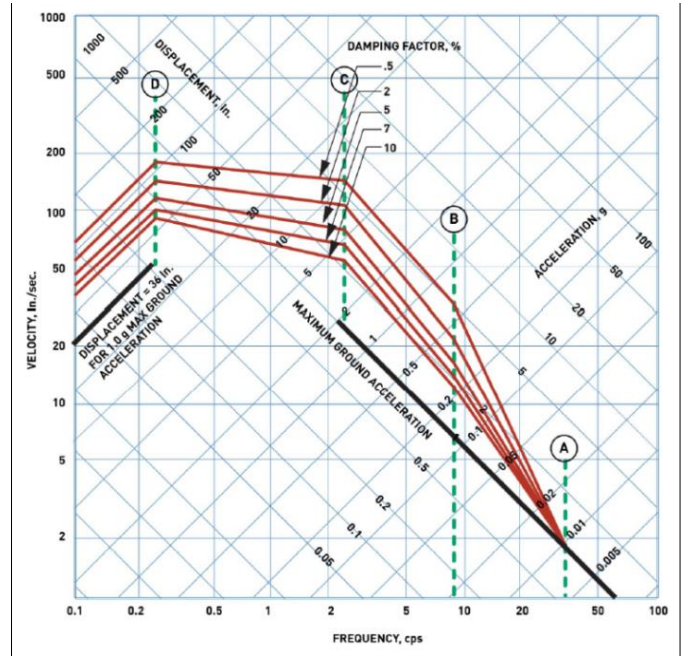


Figure (1-3). U.S. NRC Horizontal SRS_D for Nuclear Power Plants.

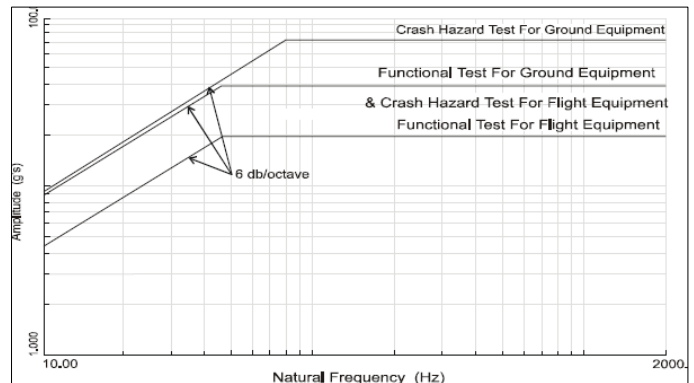


Figure (1-4). MIL-STD-810G, Method 516, Functional and Crash Hazard Shock SRS_D .

Similarly, the default SRS_D requirement for a ballistic shock environment resulting from a direct hit to a ground combat vehicle, Figure (1-5), is given by MIL-STD-810G, Method 522, Ballistic Shock⁴². This document describes the ballistic shock produced in armored vehicles for hostile attack from mines, explosives, detonation of reactive armor and projectiles. The NATO International Test Operations Procedure (ITOP) representing France, Germany, United Kingdom and the United States³⁰ has the identical SRS_D requirement for ballistic shock.

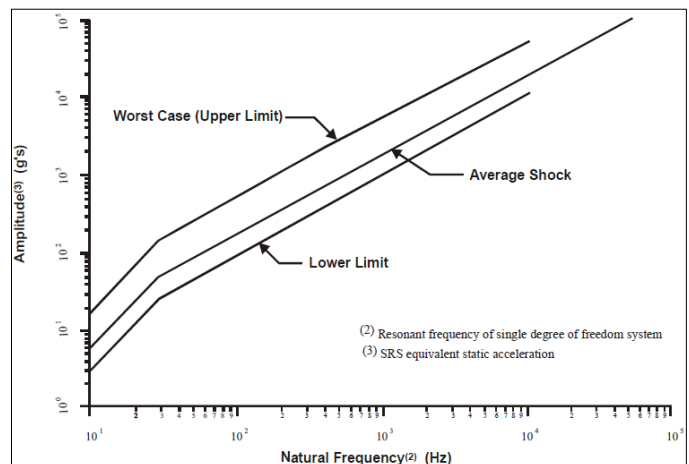


Figure (1-5). MIL-STD-810G, Method 522, Ballistic Shock SRS_D .

Pyrotechnic shock, commonly referred to as pyroshock, is the shock resulting from pyrotechnic devices which are typically an explosive or propellant activated event. A pyroshock pulse is highly localized with high acceleration and high frequency content, which can range from 300-300,000 g 's at frequencies of 100-1,000,000 Hz , and as such excite very high frequency material responses. Pyroshock sources include explosive bolts, separation nuts, pin puller, and pyro-activated operational hardware. For pyroshock, as with functional and ballistic shock, if measured data are not available, MIL-STD-810G, Method 517, Pyroshock⁴² specifies a default SRS_D for design purposes, shown in Figure (1-6). NASA also references the SRS_D of Figure (1-6)⁴⁶.

1.4 Role of a Synthesized Acceleration

As indicated in Section 1.3, the required shock design environment is frequently specified in terms of a design SRS_D . If a linear structural dynamic system is to be analyzed to SRS_D requirements, the analysis can be done directly with the mode superposition process described in Appendix A. Mode superposition is a linear process based on an Eigen value extraction from the linear equations of motion for a linear system. However, if the system has nonlinear elements such as nonlinear springs, dampers or nonlinear material properties, the resulting equations of motion are nonlinear and mode superposition is not possible because the system normal modes of vibration are not stationary.

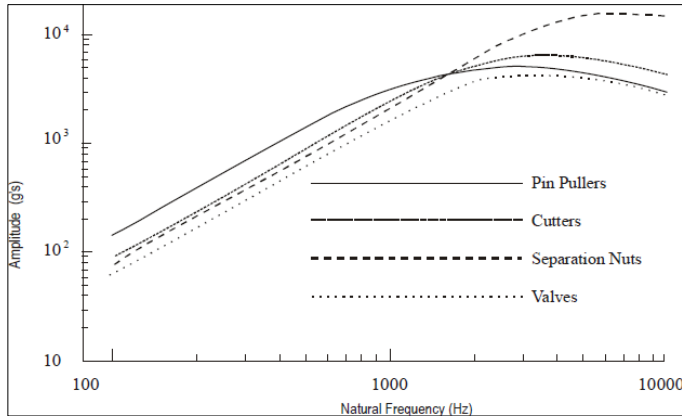


Figure (1-6). MIL-STD-810G, Method 517, Pyrotechnic Devices SRS_D .

Similarly, if a physical system is to be shock tested to SRS_D requirements, the SRS_D cannot be used directly to control the test machine. Much of the motivation to determine a synthesized a_S compatible with a design SRS_D is for shock testing with electro-dynamic shakers^{48, 59, 63}. These types of test machines have physical limitations in terms of how much force they can deliver to the test article and maximum displacement limitations of the shaker armature. The peak shaker force is based on the peak acceleration of the transient acceleration time-history and the weight of the equipment being tested (max force=mass*peak acceleration). The peak displacement limitation can also be problematic for low frequencies where the acceleration is generally low but the peak displacement is high.

In both cases of analysis or test, a synthesized SRS_D compatible shock acceleration time-history, a_S , is necessary. It is not difficult to synthesize a transient a_S with a corresponding SRS_S that matches a prescribed SRS_D within a specified tolerance envelope requirement. Many techniques exist to synthesize a shock acceleration, described in Section 2.3, based solely on matching the SRS_D with no consideration of other constraints. The assumption has been that if SRS_S from a_S matches SRS_D within prescribed tolerances, when a_S is applied to a system model or test article by analysis or test, respectively, the system response should be accurate. However, past studies have demonstrated that system responses to a synthesized base acceleration a_S can, and frequently do, vary significantly from responses to the design acceleration a_D . Additional useful information is available to mitigate this problem. This information includes the energy input to the structure from the shock acceleration and, if field test data are available, temporal information for the overall temporal shape envelope and temporal moments of the shock acceleration. However, based on published literature, others have not included this additional information in the a_S synthesis process. The energy input to the system, based on the energy input spectrum EIS , provides additional information beyond the SRS_D which can be considered in the synthesis of a_S . Further, others have not

included temporal moments as a part of the a_S synthesis process. In addition, there is a paucity of published literature where authors have verified the accuracy of the synthesized a_S based on $MDOF$ system responses relative to the corresponding responses from a known design acceleration, a_D .

1.5 IR&D Objectives

The objectives of this study are to determine a systematic method to:

- Expand the SRS compatible base acceleration synthesis process to include energy input and temporal information,
- Demonstrate improved system response from the expanded process

1.6 Report Outline

To address these objectives, an expanded approach has been developed for the synthesis of a_S . This approach broadened the current synthesis process (Section 2) to include not only SRS_D compatibility, but also compatibility with a design energy input spectrum, EIS_D , and a design temporal moments. These quantities are determined from a known design acceleration, a_D . An optimization algorithm was developed (Section 3) to return a_S which minimizes the following factors with a merit function M ,

- $SRS\%$ (average % error of SRS_S : SRS_D),
- $EIS\%$ (average % error of EIS_S : EIS_D) and
- Five Temporal Moments (% error of TM_S : TM_D).

A regression analysis was performed based on fourteen accelerations synthesized with the merit function and the corresponding $3DOF$ system responses. An optimized acceleration was synthesized with the updated merit function.

The optimized acceleration was compared with four a_S synthesized using common industry practices (classical pulse, damped sines, wavelets, enveloped sines), (Section 4). To evaluate the accuracy of the five a_S , a second $3DOF$ model was developed based on the U. S. Navy's medium weight shock machine ($MWSM$). Representative linear and nonlinear variants of the $MWSM$ model were developed. $MWSM$ model responses were determined from the five a_S . Responses evaluated were peak mass accelerations, peak displacements and peak system energy input per unit mass. The peak model responses from synthesized a_S were compared with the corresponding $MWSM$ model peak responses from a prescribed design acceleration a_D . The accuracy of each a_S was evaluated based on the $MWSM$ model responses.

1.7 Overview of Findings

Evaluation of all a_S was based on the peak responses of the $MWSM 3DOF$ models compared to the corresponding response from the design acceleration, a_D . Three $MWSM$ model responses evaluated were;

- Average % error of peak mass accelerations,
- Average % error of peak mass displacements, and
- % error of $3DOF$ peak energy input.

For the $MWSM$ model linear variant, the optimized $asyn_{427k}$ resulted in the lowest percent errors for all three responses. For the two nonlinear $MWSM$ variants, optimized $asyn_{427k}$ had lower percentage errors relative to the other four synthesized a_S , for peak mass accelerations and displacements in the majority of the cases. For all $MWSM$ model variants (linear and nonlinear), the optimized $asyn_{427k}$ resulted in the lowest peak energy input percent error. The optimized $asyn_{427k}$ was the only synthesized shock acceleration that included matching the energy input spectrum from the design acceleration, EIS_D , as a part of the optimization process.

Energy input to a system from shock acceleration represents integrating the energy equation over the entire structure, and as such is a comprehensive measure of total system damage potential. On the other hand, local displacements and accelerations cannot represent the damage potential for the entire structure and do not have general significance for the entire structure.

2 Background

2.1 Overview

Numerous methods exist to synthesize a base acceleration a_S to be compatible with a design SRS_D . Current practices focus on the singular goal of achieving the best match of SRS_S with SRS_D . However, additional information is available to augment the synthesis of a_S including the energy input per unit mass, which can be derived from the SRS_D , and temporal information that can be extracted from available test data. An overview of the common a_S synthesis methods is described herein. Derivations of the SRS and the energy input

equations are presented. Temporal information is defined including shock pulse durations and overall envelope.

2.2 Derivation of the Shock Response Spectrum

The SRS was defined and illustrated in Section 1.2 as the maximum response acceleration from a series of linear *SDOF* oscillators covering a frequency range when subjected to a common input base acceleration-time history. In this section the maximum response of each *SDOF* oscillator of circular frequency ω_n is derived. Consider a series of linear damped *SDOF* oscillators with N different natural frequencies, all mounted on a common fixed base, shown in Figure (2-1).

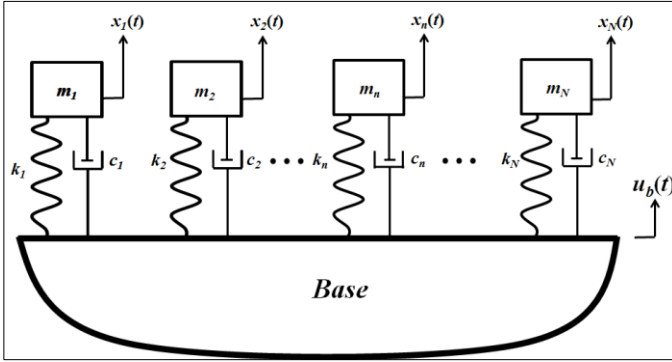


Figure (2-1). Series of *SDOF* Oscillators on a Common Base.

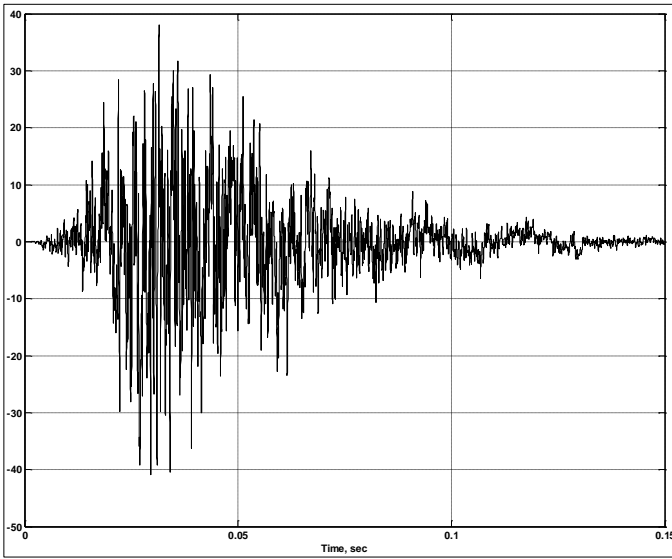


Figure (2-2). Typical Base Acceleration $\ddot{u}_b(t)$.

Each oscillator has an independent absolute coordinate, $x_n(t)$. The base coordinate is $u_b(t)$. If the base is subjected to transient shock acceleration $\ddot{u}_b(t)$ such as the one shown in Figure (2-2), this will induce an independent response in each oscillator. The governing equation of motion for the n^{th} oscillator, developed by putting m_n in dynamic force equilibrium from d' Alembert's principle, is

$$m_n \ddot{x}_n(t) + c_n (\dot{x}_n(t) - \dot{u}_b(t)) + k_n (x_n(t) - u_b(t)) = 0, \quad (2-1)$$

where $x_n(t)$ is an absolute coordinate for the displacement of the n^{th} mass m_n . A relative coordinate for the displacement of the mass relative to the base is defined for each oscillator as,

$$z_n(t) \equiv x_n(t) - u_b(t). \quad (2-2)$$

Substituting (2-2) into (2-1) yields,

$$m_n (\ddot{z}_n(t) + \ddot{u}_b(t)) + c_n \dot{z}_n(t) + k_n z_n(t) = 0. \quad (2-3)$$

Dividing by m_n and moving the base acceleration base acceleration term to the right hand side of the equation gives,

$$\ddot{z}_n(t) + \frac{c_n}{m_n} \dot{z}_n(t) + \frac{k_n}{m_n} z_n(t) = -\ddot{u}_b(t). \quad (2-4)$$

It is recognized that $\frac{k_n}{m_n} = \omega_n^2$ is the squared natural frequency of the n^{th}

oscillator and that $\frac{c_n}{m_n} = 2\zeta_n \omega_n$ is the damping term where ζ_n is the

percent of critical damping. Making these substitutions gives a *SDOF* equation of motion (2-5) in relative coordinates z_n as,

$$\ddot{z}_n(t) + 2\zeta_n \omega_n \dot{z}_n(t) + \omega_n^2 z_n(t) = -\ddot{u}_b(t). \quad (2-5)$$

From (2-1), (2-2) and (2-4), the absolute acceleration of mass m_n is determined from the relative velocity and relative displacement given by Eq. (2-6),

$$\ddot{x}_n(t) = -2\zeta_n \omega_n \dot{z}_n(t) - \omega_n^2 z_n(t). \quad (2-6)$$

The damping term is frequently ignored on the basis that the damping force contributes little to the equilibrium relationship¹³, resulting in a relationship between the absolute acceleration and the relative displacement,

$$\ddot{x}_n(t) \cong -\omega_n^2 z_n(t). \quad (2-7)$$

Eq. (2-7) indicates that the absolute acceleration of the n^{th} mass is proportional to the relative displacement between the mass and the base, with the proportionality being the squared circular frequency. The solution to Eq. (2-5) is given by Duhamel's Integral,

$$z_n(t) = -\frac{1}{\omega_n \sqrt{1-\zeta_n^2}} \int_0^t \ddot{u}_b(\tau) e^{-\zeta_n \omega_n (t-\tau)} \sin \omega_n \sqrt{1-\zeta_n^2} (t-\tau) d\tau. \quad (2-8)$$

Substituting (2-8) into (2-7) gives the absolute acceleration of mass m_n , Eq. (2-9),

$$\ddot{x}_n(t) = \frac{\omega_n}{\sqrt{1-\zeta_n^2}} \int_0^t \ddot{u}_b(\tau) e^{-\zeta_n \omega_n (t-\tau)} \sin \omega_n \sqrt{1-\zeta_n^2} (t-\tau) d\tau \quad (2-9)$$

The SRS defined as the absolute value of the peak mass accelerations over all frequencies ω_n . For the n^{th} frequency this is given by,

$$SRS_n \equiv |\ddot{x}_n(t)|_{\max}. \quad (2-10)$$

Substitution of Eq. (2-9) into (2-10) gives the SRS_n value for the n^{th} frequency *SDOF* oscillator,

$$SRS_n = \left| \frac{\omega_n}{\sqrt{1-\zeta_n^2}} \int_0^t \ddot{u}_b(\tau) e^{-\zeta_n \omega_n (t-\tau)} \sin \omega_n \sqrt{1-\zeta_n^2} (t-\tau) d\tau \right|_{\max} \quad (2-11)$$

A graph of a shock response spectrum is developed by plotting SRS_n as a

function of ω_n , or more commonly $f_n = \frac{\omega_n}{2\pi}$ in hertz, for all frequencies. A plot of the SRS for the base acceleration of Figure (2-2) is shown in Figure (2-3). Note that at the high frequency end of the plot, the SRS is approaching the 40 g asymptote which corresponds to the peak amplitude of the base acceleration in Figure (2-2).

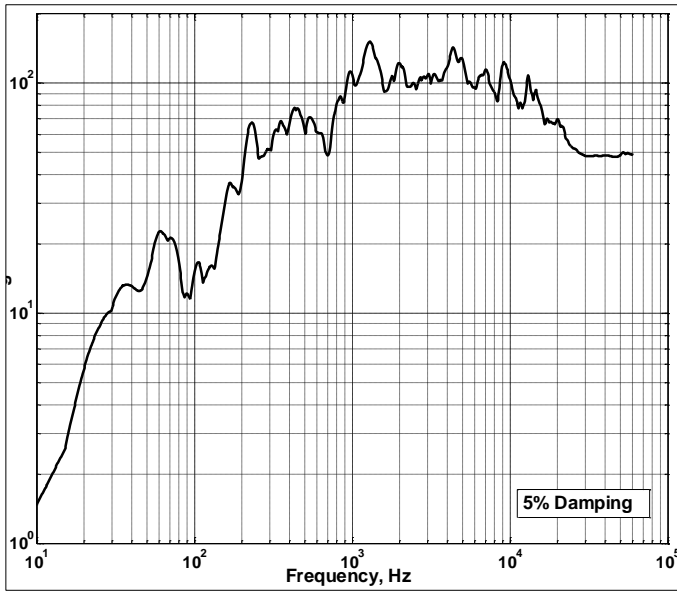


Figure (2-3). Typical Shock Response Spectrum for Mechanical Shock.

2.3 Methods to Synthesize SRS Compatible Acceleration

Early methods to synthesize spectrum compatible ground accelerations were done in the study of earthquakes by the seismic community. As early as the 1940's, Housner²⁵ modeled an earthquake as a random process with a series of pulses of different magnitudes that occurred randomly in time. Subsequently, Housner²⁶ used a technique of modeling an earthquake as the sum of sine wave pulses occurring randomly in time, with frequency and amplitude determined from a probability distribution.

Additional research to synthesize an SRS compatible acceleration time-history was continued in the 1960's by the seismic community. Civil engineers recognized the need to model ground structures analytically to determine the survivability to withstand strong earthquakes. Early methods to synthesize base accelerations compatible with a prescribed design SRS_D were approached by modifications of earthquake acceleration records. These approaches were to use either stationary random processes^{28, 35, 52, 54, 58} or non-stationary random processes^{33, 34, 55} to guide the modification of earthquakes acceleration data for the synthesis of an artificial earthquake. The approach was to choose a starting set of coefficients for each frequency of SRS_D and modify the set iteratively to improve the agreement between the SRS_S of the artificial earthquake and the SRS_D of the real earthquake⁵³. Several starting procedures were explored including:

- Selection of an existing earthquake acceleration record which had an SRS that was close to the target SRS_D ,
- Selection of an initial set of coefficient by modification of the amplitude of the Fourier transform of the existing earthquake and
- Modification of the power spectral density (PSD) of the real earthquake for the set of coefficients for each frequency.

During the 1970's, procedures to synthesize SRS_D compatible acceleration time-histories emerged which did not rely on existing earthquake acceleration data records. These methods employed the summation of sinusoids using a temporal envelope function to control the rise and decay of the synthesized acceleration^{1, 20, 22, 36, 39, 56}.

The introduction of neural networks in the 1990's provided seismic engineers other methods to synthesize spectrum compatible ground accelerations. One such method was to train a two stage neural network from 30 earthquake ground acceleration records²¹. Another approach employed a five neural network model to synthesize an SRS_D compatible ground acceleration³⁸. This approach used basic earthquake information such as magnitude, epicenter distance, site conditions and focal depth to train the neural networks. While neural network based processes did result in a synthesized earthquake acceleration, limitations existed based on departure of the earthquake of interest compared to those that trained the neural networks. In general the match of the synthesized SRS_S was not particularly accurate to the target SRS_D .

Soize⁶⁴ published a unique method to synthesize a_S to be compatible with SRS_D using the maximum entropy principal. This principle was used to construct the probability distribution of a non-stationary stochastic process.

The resulting a_S waveform appeared credible and the agreement between SRS_S and SRS_D was reasonable.

Brake⁹ published an interesting approach of combining different basis functions to synthesize an SRS compatible base acceleration. These functions were impulses, sines, damped sines and wavelets. With various combinations of these functions and optimizing the coefficients of each with a genetic algorithm, Brake was able to obtain a reasonable match of SRS_S and SRS_D . The resulting transient a_S wave form, however, was obviously a "manufactured" time-history with little temporal relation to real test data.

Others in the seismic community continued to explore the synthesis of SRS compatible ground acceleration time-histories using the stationary and non-stationary features of earthquakes to include the power spectral density function^{23, 72}.

Presently for mechanical shock, the most common techniques to synthesize an SRS compatible acceleration a_S are:

- classical pulse (e.g. half-sine, terminal peak saw-tooth, trapezoid),
- damped sinusoids,
- wavelets and
- enveloped sinusoids.

MIL-STD-810G, Method 516¹⁵ specifies that if test data are not available, the use of damped or amplitude modulated sinusoids is permissible provided that the SRS_S exceeds a prescribed SRS_D over a frequency range of 5-2000 Hz. The use of a classical pulse (either terminal peak saw-tooth or trapezoid), while

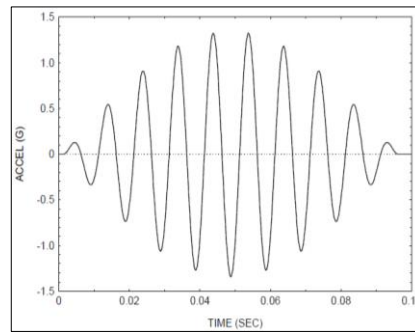


Figure (2-4). Individual Wavelet Example.

is the least desirable approach, is permitted if no test data are available. The UK MOD⁴³ also imposes requirements and tolerances on pulses (half sine, terminal peak saw-tooth, and trapezoidal) and damped sinusoids in terms of peak amplitude and number of shocks pulses.

Beyond classical shock pulses to synthesize an SRS_D compatible a_S , some variant of the summation of sinusoids is the most frequently used method for mechanical shock. One method, especially relevant for control an electro-dynamics shaker test machine, is wavelets³¹. Multiple discrete wavelets, when summed, will result in a synthesized a_S wave form. A discrete wavelet has a sinusoidal motion with a finite and specific number of half sine oscillations with unique parameters for frequency, amplitude and time delay. Iterations for the parameters of each wavelet yield a synthesized a_S with a resulting SRS_S that matches SRS_D within acceptable tolerances. The equation for an individual wavelet, $W_n(t)$, is given by,

$$W_n(t) = 0 \quad t < t_{dn} \quad (2-12)$$

$$W_n(t) = A_n \sin\left\{\frac{\omega_n}{N_n}(t-t_{dn})\right\} \sin\left\{\omega_n(t-t_{dn})\right\} \quad t_{dn} \leq t \leq \left(t_{dn} + \frac{N_n\pi}{\omega_n}\right) \quad (2-13)$$

$$W_n(t) = 0 \quad t > \left(t_{dn} + \frac{N_n\pi}{\omega_n}\right) \quad (2-14)$$

$$a_S(t) = \sum_{n=1}^N W_n(t) \quad (2-15)$$

where,

- $W_n(t)$ is the acceleration of wavelet n at time t ,
- A_n is the wavelet amplitude,
- N_n is the number of half-sines in the wavelet (odd integer ≥ 3),
- ω_n is the wavelet frequency and
- t_{dn} is the wavelet time delay.

The complete synthesized a_S is obtained from the summation of all wavelets. An individual wavelet example is shown in Figure (2-4) where $A_n=1.34$, $f_n=100$ Hz, $N_n=19$ half-sines and $t_{dn}=0$.

Other methods to synthesize a_S are with damped and enveloped sinusoids. These approaches are similar to that of wavelets. The primary difference is the way in which the rise, peak and decay of the overall waveform is controlled. In

the case of damped sinusoids, as with wavelets, individual sinusoidal pulses are summed. Each individual damped sine pulse has a unique time delay t_{dn} , damping ζ_n , amplitude A_n , and frequency ω_n defined by,

$$W_n(t) = 0, \quad t < t_{dn}, \quad (2-16)$$

$$W_n(t) = A_n e^{-\zeta_n \omega_n (t-t_{dn})} \sin\{\omega_n (t-t_{dn})\} \quad t \geq t_{dn} \quad \text{and} \quad (2-17)$$

$$a_s(t) = \sum_{n=1}^N W_n(t). \quad (2-18)$$

An example of an individual damped sine pulse is shown in Figure (2-5) where $A_n=1.34g$, $f_n = 100 \text{ Hz}$, $\zeta=0.05$ and $t_{dn} = .01$ seconds.

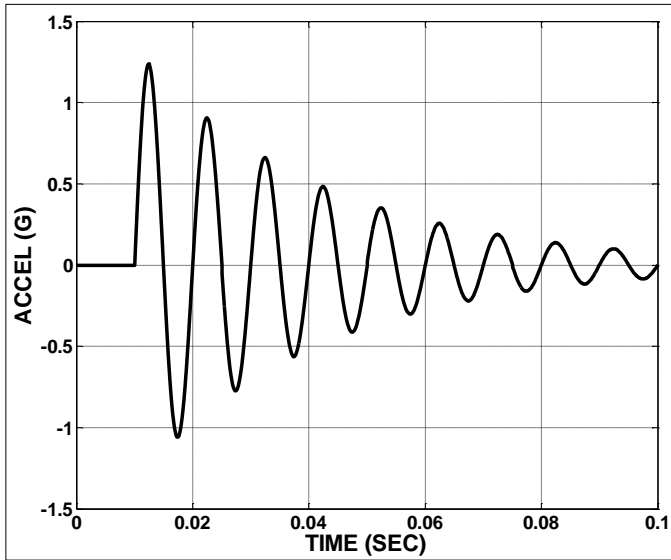


Figure (2-5). Individual Damped Sine Example.

The enveloped sinusoids with random phase angles approach is similar to damped sinusoids. The equation for enveloped sinusoids is given by,

$$a_s(t) = E(t) \sum_{n=1}^N A_n \sin(\omega_n t + \phi_n) \quad (2-19)$$

where A_n are the amplitude coefficients, ω_n are the frequencies of the sinusoids and ϕ_n are random phase angles for each frequency n . The rise, plateau and decay of a_s is controlled by an envelope function $E(t)$ rather than damping. Since $E(t)$ can be sized to any temporal shape needed, the synthesized pulse shape of a_s can be closely controlled to match that of available test or design data. Figure (2-6) is a plot of $E(t)$ superimposed on the enveloped sinusoids synthesized acceleration time-history a_s . Inasmuch as $E(t)$ is sized to control the relative rise, plateau and decay of a_s , the value of the plateau is commonly set to unity. However, $E(t)$ was increased by a factor of 40 in Figure (2-6) to better illustrate the relationship of $E(t)$ to the corresponding shape of a_s . The transient pulse is developed as the summation of sinusoids of amplitude A_n over n frequencies needed to span the frequency bandwidth of interest. During each iteration i of the synthesis process, the amplitude coefficients A_n are adjusted to improve the agreement of SRS_S with SRS_D . The updated A_n coefficients are adjusted during each iteration for each frequency n from,

$$A_n^{i+1} = \frac{SRS_D^n}{(SRS_S^n)^{1/2}} A_n^i$$

Figure (2-7) is a plot of the design acceleration a_D and four accelerations (half sine, damped sines, wavelets and enveloped sines) synthesized to match SRS_D . No attempt was made to match the energy input spectrum or temporal moments of a_D . The time scale of the half sine pulse was expanded by a factor of ten relative to the others in Figure (2-7), to better show the shape of the synthesized waveform. The SRS_S of the synthesized accelerations, with the exception of the half sine, matched SRS_D with good agreement. Figure (2-8) shows SRS_D and SRS_S for the four synthesized a_s . Table (2-1) is the percentage errors for the SRS_S of the synthesized accelerations relative to SRS_D . The percentage error for each is the percent difference between SRS_S and SRS_D

averaged over all the frequencies. The error was least for enveloped sines at 4.88%.

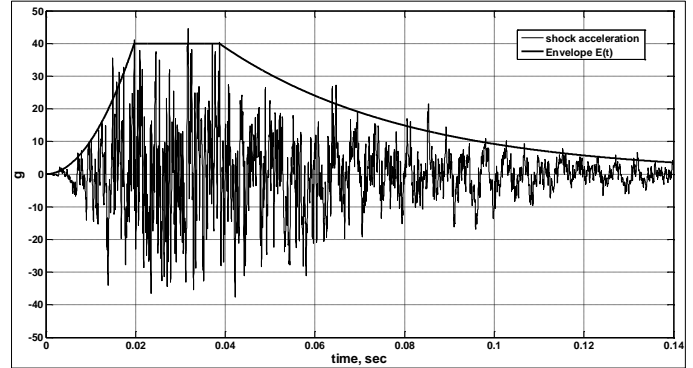


Figure (2-6). Envelope $E(t)$ Superimposed on Corresponding Enveloped Sinusoids a_s

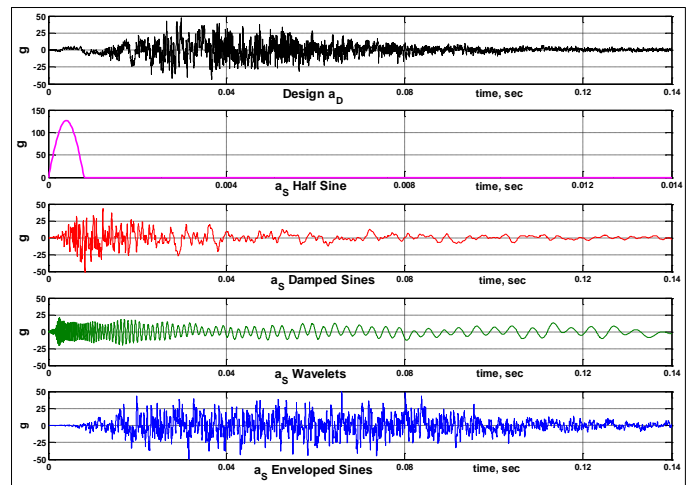


Figure (2-7). Design a_D and Synthesized Accelerations.

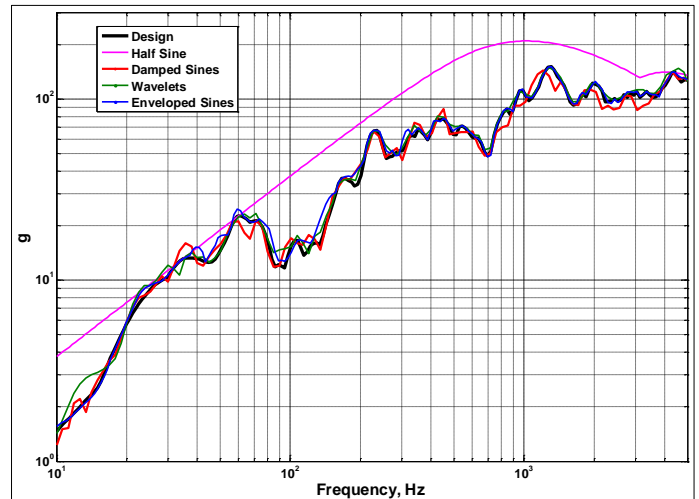


Figure (2-8) Design SRS_D and SRS_S of Synthesized Accelerations.

Table (2-1). Synthesized Accelerations SRS_S % Error.

	Average SRS_S % Error
Half Sine	83.3%
Damped Sines	8.67%
Wavelets	6.97%
Enveloped Sines	4.88%

As demonstrated in Figure (2-8), it is not difficult to synthesize a base acceleration a_s that matches a prescribed design SRS_D within specified tolerance limits, such as $\leq 10\%$ error. However, past research by Alexander² has indicated that to obtain an accurate response from a structural dynamic model, matching only the SRS_D is not sufficient. While a specific base acceleration transient will result in a unique shock response spectrum, the inverse is not true. There are theoretically an infinite number of base accelerations that will yield the same SRS . The phasing of the modes of a structural dynamic model relative to the timing of the synthesized acceleration peaks can significantly affect peak $MDOF$ response magnitudes. The goal of the research herein is to determine a process, with additional guidelines beyond common practices, that will yield not only a spectrum compatible synthesized base acceleration, but also will yield improved results when applied to linear and nonlinear physical system models, especially for energy input. To improve the accuracy of a physical system model response to a_s , additional constraints are explored for the acceleration synthesis process. One such constraint is temporal (time) moments of the synthesized transient acceleration pulse. If test data have been acquired, temporal information can be determined from the data set to guide the synthesis of a_s .

2.4 Evolution of Energy Methods for Shock and Vibration

Research of energy methods for transient shock response modeling provides another constraint to be applied in the synthesis of a_s . This involves compatibility with not only the SRS_D , but also with the EIS_D . Synthesis of a_s to be compatible with SRS_D , EIS_D and temporal moments offer additional constraints to be considered for the objective of improving $MDOF$ system response accuracy.

The seismic community did much of the early research to examine the utility of base acceleration energy input. The use of energy to characterize base excited structural dynamic response dates back to Hudson²⁹ and Housner²⁷. Hudson documented the maximum energy per unit mass for a $SDOF$ oscillator is given by relationship to the velocity shock response spectrum,

$$\frac{\text{max energy}}{\text{unit mass}} = \frac{1}{2} SRS_{vel}^2 \quad (2-20)$$

Hudson further developed a relationship between the velocity spectrum and the total energy from a series of pulses similar to that of earthquake excitation. Housner derived a relationship for the average energy in a $MDOF$ structure based on the superposition of the total modal energies for each of the normal modes of the structure. The average energy in the structure for a transient shock is given as a function of the total mass of the structure and the average of the squared velocity spectral value of all N normal modes of the structure,

$$\text{Energy}_{ave} = \frac{1}{2} M (SRS_{vel_n}^2)_{ave} \quad (2-21)$$

Other authors who have documented the relationship between energy and the square of the velocity spectrum include Edwards et al.^{17, 68, 71}.

Shock motion can be characterized by energy delivered to a structure. It is possible to determine energy input from a base acceleration-time history, and from the conservation of energy, the input energy will balance the energy from system response. The EIS is similar to an SRS inasmuch as it is a frequency based measure of the response of a series of $SDOF$ oscillators subjected to a common base acceleration. However, in the case of an EIS , the measure is peak energy input per unit mass to the $SDOF$ oscillator from the base acceleration, instead of peak mass acceleration response as in the case of the SRS . As with the SRS , peak energy input is determined for a series of $SDOF$ oscillators covering the frequency bandwidth of interest. Derivation of the EIS is in developed Section 2.5.

As was the case for the SRS , much of the ground work to study base excitation of a structure in terms of energy, in general, and the development of the EIS , in particular, was done by the seismic community from the mid-1980's to the present. Zahrah and Hall⁷¹ investigated the response of simple $SDOF$ structures from strong earthquake excitations. Eight earthquakes records of magnitudes 4.7 to 7.7 were selected for representative strong ground input motions. The objective of the study was to better quantify factors that influence structural deformation and damage. The approach of the study was to compare the input energy to the dissipated energy by inelastic deformations and damping, to establish an improved damage criteria than peak ground acceleration or the shock response spectrum. The conclusion of the study was

that a better damage potential might be defined in terms of the energy input to the structure.

Two formulation of the energy input equation are possible, based on absolute and relative coordinates for the $SDOF$ equation of motion. The relative energy equation is given by Eq. (2-28). The absolute energy equation is based on derivation of the energy terms from the $SDOF$ equation of motion prior to making the substitution for the relative coordinate ($z=u-u_b$). The absolute formulation leads to the energy input term ($EI_{abs} = \int m \ddot{u} du_b$). Uang and Bertero⁶⁸ used the absolute energy formulation to compare the results of the input energy per unit mass from the $SDOF$ EIS with that of a linear multi-story building. The result was the energy input of the $SDOF$ model, on a per unit mass basis, provided a very good estimate of the input energy of the multi-story building for the dominant frequency.

Manfredi⁴¹ noted that the input energy EI is an effective tool in seismic design and represents a "very stable parameter." For the response of a nonlinear $SDOF$ system, Manfredi proposed a modification to Housner's input energy per unit mass assumption for an undamped system given by $1/2$ of the pseudo-velocity squared,

$$\left(\frac{EI}{M} \right)_{\text{max}} = \frac{1}{2} \left(\frac{SRS(\omega)}{\omega} \right)_{\text{max}}^2 \quad (2-22)$$

Manfredi's modification to Housner's equation included the addition of a second term with a dimensionless index I_D to account for the influence of the duration of the ground acceleration,

$$\left(\frac{EI}{M} \right)_{\text{max}} = 0.45 \left(\frac{SRS(\omega)}{\omega} \right)_{\text{max}}^2 + 0.10 I_D \left(\frac{SRS(\omega)}{\omega} \right)_{\text{max}} \quad (2-23)$$

Ordaz, et al.⁵¹ derived another method to determine the relative input energy per unit mass using the Fourier amplitude spectrum and the real part of the relative velocity transfer function. The relative input energy per unit mass of an $SDOF$ oscillator, derived in Section 2.5, is given by,

$$\frac{EI}{m} = - \int \ddot{u}_b(t) \dot{z}(t) dt \quad (2-24)$$

The transfer function of the base acceleration to relative velocity $\dot{z}(t)$ in the frequency domain is given by,

$$H_v(\omega, \omega_n, \zeta) = - \frac{i\omega}{\omega_n^2 - \omega^2 + 2i\zeta\omega\omega_n} \quad (2-25)$$

The Fourier spectrum of the base acceleration is given by $\ddot{u}_b(\omega)$. The resulting expression for the energy input per unit mass is given by,

$$\frac{EI}{m} = - \frac{1}{\pi} \int_0^\infty |\ddot{u}_b(\omega)|^2 \text{Re} |H_v(\omega, \omega_n, \zeta)| d\omega \quad (2-26)$$

Initial research and development for the use of energy methods was done almost exclusively by the seismic community to characterize shock damage from earthquakes. More recently other authors have published research in the application of energy methods to characterize mechanical shock as an alternative to the SRS . Authors who have considered energy methods for damage potential to mechanical systems include Gaberson¹⁹, Edwards¹⁷, Iwasa and Shi³², and Alexander⁴.

Gaberson¹⁹ was a passionate advocate for the velocity shock response spectrum, SRS_{vel} , as a measure of damage potential. One of Gaberson's arguments for the use of the SRS_{vel} was the relationship to energy ($1/2 m SRS_{vel}^2$), first noted by Hudson²⁹.

Iwasa and Shi³² advocated the maximum total energy spectrum as the best measure of damage potential in the context of pyroshock, and noted that past studies indicated that maximum acceleration does not consistently represent the most accurate measure of damage potential. Their conclusion was that the maximum energy per unit mass of an $SDOF$ system is a suitable indicator of pyroshock damage potential. This was confirmed by two mechanical tests, one from impact and one from electro-dynamic shaker input.

Based on a numerical simulation, Edwards¹⁷ demonstrated that the maximum energy input per unit mass input to a $MDOF$ structure can be estimated by the energy input per unit mass of an $SDOF$ system (i.e. the EIS) with the same frequency of the lowest (dominant) frequency of the $MDOF$ structure. Uang

and Berto⁶⁸ demonstrated a similar finding. Edward's simulation consisted of five nonlinear 4DOF systems with the pre-yield fundamental frequencies of 10 Hz, 285 Hz, 1716 Hz, 7,357 Hz and 19,739 Hz. In all five cases, the energy input per unit mass of the 4DOF structure matched the EIS at those same frequencies with good agreement.

Alexander⁴ published a study comparing the EIS from two base accelerations with the maximum energy per unit mass from the response of a 6DOF ABAQUS¹⁴ model, for both linear and nonlinear versions of model. The maximum energy per unit mass comparison from the model had good agreement with the EIS for the linear model. The same comparison for the nonlinear version of the model, while not unreasonable, had mixed results depending on the frequency.

Honeywell²⁴ was able to successfully use the EIS to quantify the total damage potential from packaging, handling and vibration from two different Honeywell operations. The EIS was developed for each of the two sites from data collected for each packaging configuration and each mode of transportation. Hartwig noted that the benefit of the EIS was that it accounts for the duration of the events and repeated exposures, where the power spectral density (PSD) does not. The same issue exists with the SRS.

2.5 Derivation of the Energy Input Equations

As with the SRS, it is possible to determine an Energy Input Spectrum (EIS), from a base acceleration from the peak energy inputs to a series of SDOF oscillators of different frequencies. A series of linear damped SDOF oscillators mounted to a common base, Figure (2-1), is also applicable for development of an EIS. Eq. (2-3) is the equation of motion of the n^{th} SDOF oscillator mounted to the base, formulated in terms of the relative coordinates z_n . Moving the inertial force term $m_n \ddot{u}_b(t)$ to the right hand side gives the equation of motion (2-27) for the n^{th} mass,

$$m_n \ddot{z}_n(t) + c_n \dot{z}_n(t) + k_n z_n(t) = m_n \ddot{u}_b(t) \quad (2-27)$$

Each term of Eq. (2-27) has units of force. To convert this equation from a force balance to an energy balance, each term is multiplied by an incremental displacement dz and integrated with respect to z , leading to the energy balance Eq. (2-28) in relative z coordinates,

$$\int m_n \ddot{z}_n(t) dz + \int c_n \dot{z}_n(t) dz + \int k_n z_n(t) dz = - \int m_n \ddot{u}_b(t) dz \quad (2-28)$$

The individual terms of on the left hand side of Eq. (2-28) describe the different forms of energy that are present in the SDOF oscillator. The right hand side of (2-28) is the input energy to the SDOF oscillator from the base acceleration. The terms on the left had side of (2-28) are kinetic, damped and absorbed energy, respectively. These terms are further expanded as follows.

Kinetic Energy,

$$\int m \dot{z} dz = \int m \frac{dz}{dt} dz \frac{dt}{dt} = \int m \dot{z} dz = \frac{1}{2} m \dot{z}^2 \quad (2-29)$$

Damped Energy,

$$\int c \dot{z} dz = \int c \dot{z} \frac{dz}{dt} dt = c \int \dot{z}^2 dt \quad (2-30)$$

Absorbed Energy, and

$$\int k z dz = \frac{k z^2}{2} \quad (2-31)$$

Input Energy:

$$- \int m \ddot{u}_b dz = - \int m \ddot{u}_b dz \frac{dt}{dt} = - m \int \ddot{u}_b \dot{z} dt \quad (2-32)$$

The kinetic energy term gives the instantaneous kinetic energy of the SDOF_n at the current time t from $\frac{1}{2}$ the product of mass and velocity squared. The damped energy term is cumulative and builds during the shock transient. The absorbed energy term for a linear spring (k =constant) becomes the instantaneous energy of $\frac{1}{2} k z^2$. In the general case where there is inelastic behavior of the spring (e.g. elasto-plastic) the absorbed energy would be cumulative during the transient due to plastic strain. Eq. (2-32) gives the input energy to the SDOF_n from the base acceleration and relative velocity. The input energy is cumulative for the duration of the shock transient. For any instance in time, the input energy is equal to the sum of the response energy

terms on the left hand side of Eq. (2-28). An updated energy equation for the motion of a linear SDOF_n oscillator is given by Eq. (2-33),

$$\frac{1}{2} m_n \dot{z}_n(t)^2 + c_n \int \dot{z}_n(t)^2 dt + \frac{1}{2} k_n z_n(t)^2 = - m_n \int \ddot{u}_b(t) \dot{z}_n(t) dt \quad (2-33)$$

Figure (2-9) is an example of the individual transient energies and the total transient input energy for a 10 Hz SDOF oscillator from a base acceleration. It is apparent from observation of the figure that the sum of the individual energy terms on the left hand side of Eq. (2-33) are equal to the input energy on the right hand side of Eq. (2-33) at every instance in time.

If the peak values of the input energy term, right hand side of Eq. (2-33), are plotted as a function of frequency for all N SDOF systems, an energy input spectrum is determined. Figure (2-10) shows the energy input from transient design base acceleration $\ddot{u}_b(t)$ for three SDOF oscillators tuned to frequencies of 10 Hz, 100 Hz and 1,000 Hz. The corresponding peak input energy per unit mass values are 159.6 in²/sec², 74.5 in²/sec² and 67.6 in²/sec², respectively. These points are indicated by a square, an ellipse and a circle, respectively, in Figure (2-10). These peak energy input amplitudes are the magnitudes of the EIS for transient base acceleration at the corresponding frequencies, also indicated by a square, an ellipse and a circle, respectively, in Figure (2-11). The complete EIS for the base acceleration $\ddot{u}_b(t)$ covering frequency bandwidth of 10 Hz to 5,000 Hz is plotted in Figure (2-11).

Derivation of an energy equation for a MDOF structure is similar to that of a SDOF oscillator, and modifications to the MDOF matrix equation of motion are also similar to that of the SDOF scalar equation of motion. For a linear MDOF system in relative coordinates, the matrix equation of motion is given by Eq. (2-34),

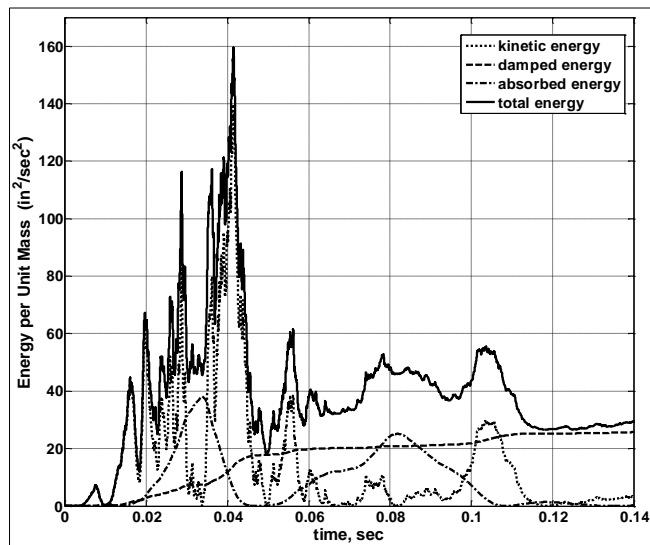


Figure (2-9). Transient Energy Input for 10 Hz SDOF.

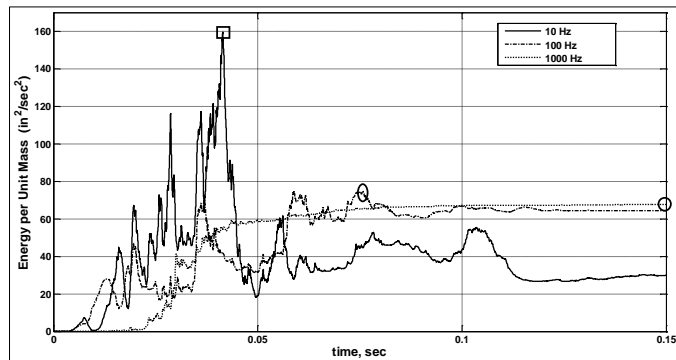


Figure (2-10). Base Acceleration $\ddot{u}_b(t)$ Transient Energy Input for Three SDOF Oscillators.

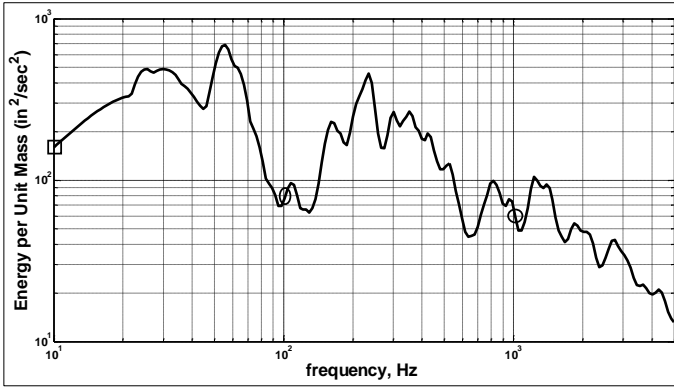


Figure (2-11). Base Acceleration $\ddot{u}_b(t)$ Energy Input Spectrum (EIS).

$$[M]\{\ddot{z}\} + [C]\{\dot{z}\} + [K]\{z\} = -[M]\{1\}\ddot{u}_b \quad (2-34)$$

To convert Eq. (2-34) to from a force balance to an energy balance, we again multiply each term by $\{dz\}^T$ and integrate with respect to z , leading to the *MDOF* energy Eq. (2-35),

$$\int \{dz\}^T [M]\{\ddot{z}\} + \int \{dz\}^T [C]\{\dot{z}\} + \int \{dz\}^T [K]\{z\} = - \int \{dz\}^T [M]\{1\}\ddot{u}_b \quad (2-35)$$

Noting that $\{dz\}$ can be rewritten as $\left\{\frac{dz}{dt}\right\} dt$, this substitution in (2-35)

for all terms, except the absorbed energy term results in,

$$\int \{\dot{z}\}^T [M]\{\ddot{z}\} dt + \int \{\dot{z}\}^T [C]\{\dot{z}\} dt + \int \{dz\}^T [K]\{z\} = - \int \{\dot{z}\}^T [M]\{1\}\ddot{u}_b dt. \quad (2-36)$$

If similar transformations are executed for (2-36) as was done for the *SDOF* energy terms, Eq. (2-29) through Eq. (2-32), the same energy terms occur for the *MDOF* system, given by,

$$\text{Kinetic Energy: } \frac{1}{2} \{\dot{z}\}^T [M]\{\dot{z}\} \quad (2-37)$$

$$\text{Damped Energy: } \int \{\dot{z}\}^T [C]\{\dot{z}\} dt, \quad (2-38)$$

$$\text{Absorbed Energy: and } \frac{1}{2} \{z\}^T [K]\{z\} \quad (2-39)$$

$$\text{Input Energy: } - \int \{\dot{z}\}^T [M]\{1\}\ddot{u}_b dt. \quad (2-40)$$

For the *3DOF* system models described in Chapters 3 and 4, the input energy was computed from Eq. (2-40). The time integration was performed using the central difference numerical integration time stepping routine, where the dynamic analysis is executed by stepping through the transient with equal Δt time increments. The integration procedure evaluates the incremental ΔE_n^k input energy for current time step increment k , and adds ΔE_n^k to the cumulative sum of all prior time steps, E_n^{k-1} . The *3DOF* energy input time stepping procedure is,

$$E_n^k = E_n^{k-1} + \Delta E_n^k, \quad (2-41)$$

$$E_n^k = E_n^{k-1} - \begin{bmatrix} \dot{z}_1 & \dot{z}_2 & \dot{z}_3 \end{bmatrix}^k \begin{bmatrix} m_1 & 0 & 0 \\ 0 & m_2 & 0 \\ 0 & 0 & m_3 \end{bmatrix} \begin{Bmatrix} 1 \\ 1 \\ 1 \end{Bmatrix} \ddot{u}_b^k \Delta t \text{ and} \quad (2-42)$$

$$E_n^k = E_n^{k-1} - (m_1 \dot{z}_1 + m_2 \dot{z}_2 + m_3 \dot{z}_3) \ddot{u}_b^k \Delta t. \quad (2-43)$$

2.6 Temporal Information from a Shock Acceleration

In addition to the *SRS* and *EIS*, if temporal information is available from shock test data it offers additional information for the synthesis of a_s . Temporal characteristics of a typical shock acceleration time-history include the overall envelope shape and temporal moments. Temporal moments quantify the shape of the shock pulse including the centroid, duration, relative rise/decay and the degree of concentration about the centroid.

The envelope $E(t)$ is the relative temporal shape of the overall rise, plateau and decay of the shock acceleration time-history. Since $E(t)$ is a relative shape of the shock acceleration, the plateau is typically set to 1.0. For a family of test data, $E(t)$ can be determined based on a best fit of the data. Although various shapes are possible, mechanical shock acceleration is frequently characterized by a rapid exponential rise, a relative short plateau region, followed by a more gradual exponential decay. $E(t)$ has the same characteristics. A typical shock $E(t)$ envelope used to control the overall rise and decay of the enveloped sinusoids synthesized acceleration as is plotted in Figure (2-6).

Smallwood⁶⁰⁻⁶² proposed the use of bandlimited temporal moments to characterize shock accelerations. Smallwood noted that the *SRS* was developed to reduce a complex base acceleration time-history to a simple representation, based on the peak response of a series of *SDOF* oscillators as described in Section 1.2. However as noted in Section 1.4, an *SRS* compatible time-history is needed for structural analysis of a nonlinear system model and also for electro-dynamic shaker shock testing. A serious limitation of the *SRS* is that it contains no information about the duration of shape (rise and decay time) of the shock event. Further, the actual shock event is usually oscillatory, but frequently a simple unidirectional wave form pulse is used for shock testing such as the half-sine pulse described in Section 2.3. As shown in Figure (2-7) this can lead to a very short duration wave form with significantly higher peak amplitude than the data, which can lead to a serious over test condition. Another limitation of the *SRS* is that it has no spectral content.

The use of band limited temporal moments can mitigate some of these limitations when synthesizing an *SRS* compatible acceleration. A brief description of temporal moments is contained herein. The reader is referred to the Smallwood references for an in depth description. The i^{th} temporal moment $m_i(\varepsilon)$ of a time-history $a(t)$ about a time location ε is defined to be,

$$m_i(\varepsilon) = \int_{-\infty}^{\infty} (t - \varepsilon)^i a^2(t) dt. \quad (2-44)$$

Temporal moments are useful to characterize the time-history temporal characteristics of a complex shock wave form. Temporal moments are analogous to probability density functions. The square of the time history is used for several reasons including avoidance of negative amplitudes. The first five temporal moments are given specific names. The zero order temporal moment, Eq. (2-45), is called energy (E) but in general will not have energy units. Note from (2-45) that energy E is independent of ε .

$$E = m_0(\varepsilon) = \int_{-\infty}^{\infty} a^2(t) dt. \quad (2-45)$$

If the centroid of $a(t)$ occurs at time $t = \tau$, the first moment about τ is zero.

$$m_1(\tau) = \int_{-\infty}^{\infty} (t - \tau) a^2(t) dt = 0. \quad (2-46)$$

From Eq. (2-45) and (2-46) it can be shown that,

$$\tau = \frac{m_1(a)}{m_0(a)}. \quad (2-47)$$

The next three temporal moments are taken about the centroid τ . Moments taken about time $t = \tau$ are termed central moments. The centroid avoids the problem of having the temporal moments depend on the choice of the time origin. These three moments are of particular interest and are designated as *RMS* duration, skewness and kurtosis, respectively. The square root of the second central moment, normalized by energy is the *RMS* duration, D . This duration is analogous to the moment of inertia in mechanics or standard deviation of random numbers.

$$D^2 = \frac{m_2(\tau)}{E} = \frac{1}{E} \int_{-\infty}^{\infty} (t - \tau)^2 a^2(t) dt. \quad (2-48)$$

Skewness is a measure of the relative rise and decay time of $a(t)$. Mechanical shock typically has a rapid rise time with a more gradual decay time, which results in positive skewness. A symmetric waveform results in zero skewness. Skewness S normalized by duration is given by Eq. (2-50).

$$S_t^3 = \frac{m_3(\tau)}{E} = \frac{1}{E} \int_{-\infty}^{\infty} (t - \tau)^3 a^2(t) dt, \quad (2-49)$$

$$S = \frac{S_t}{D}. \quad (2-50)$$

Kurtosis is a measure of the central tendency of the waveform. For example high kurtosis may represent a bimodal pulse. Low kurtosis indicates the waveform is concentrated near the centroid. Kurtosis K normalized by duration is given by Eq. (2-52).

$$K_t^4 = \frac{m_4(\tau)}{E} = \frac{1}{E} \int_{-\infty}^{\infty} (t - \tau)^4 a^2(t) dt, \quad (2-51)$$

$$K = \frac{K_t}{D}. \quad (2-52)$$

Smallwood (1989) notes that the importance of skewness and kurtosis relative to the response of a system is not obvious, and that matching the centroid and RMS duration is clearly more important. The square root of E normalized by the RMS duration is termed the root energy amplitude (REA), which conveniently has the same units as $a(t)$, which is acceleration in this case. REA provides a convenient way to describe the energy of the shock pulse.

$$REA = \sqrt{E/D}. \quad (2-53)$$

Figure (2-12) is a plot of the design acceleration a_D with the temporal moments indicated on the plot, including the magnitude of the root energy amplitude plotted at the centroid τ .

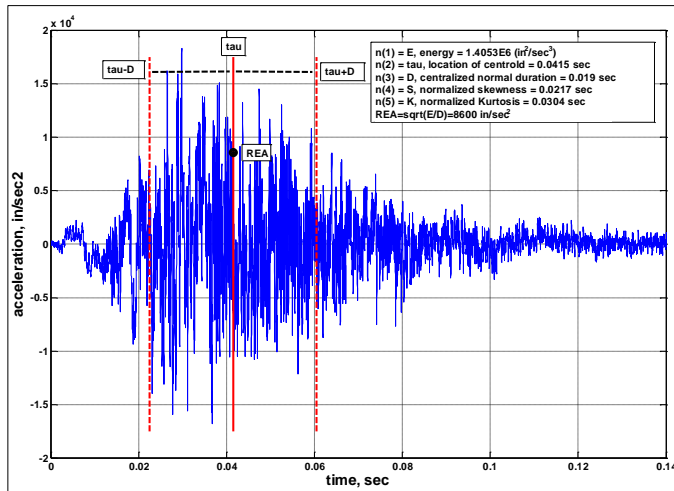


Figure (2-12). Design Shock Acceleration a_D with Temporal Moments.

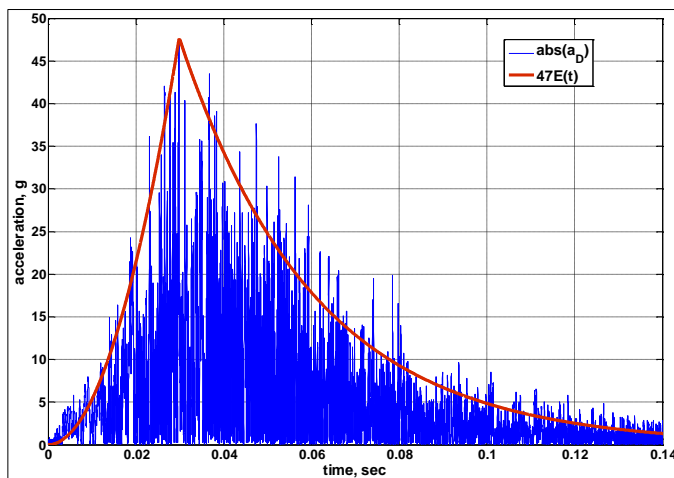


Figure (2-13). Design Acceleration $|a_D|$ and Envelope $E(t)$.

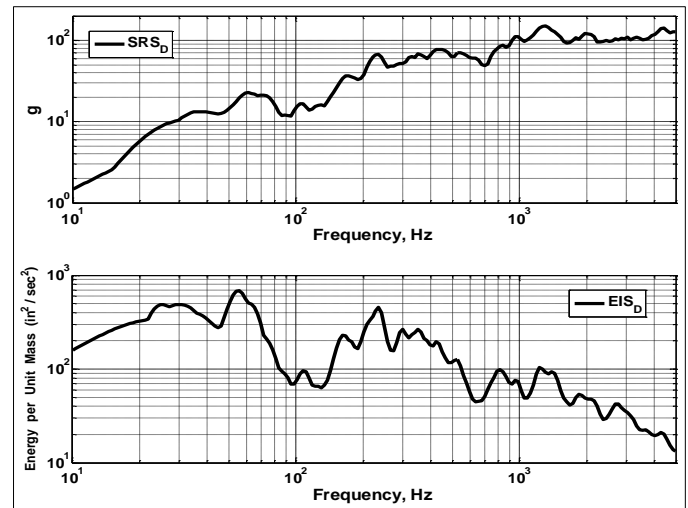


Figure (2-14). Design SRS_D and EIS_D .

2.7 Define Baseline a_D , SRS_D , EIS_D and Temporal Moments for Present Study

Previously in this document, references have been made to a design acceleration a_D and the corresponding design shock response spectrum SRS_D . For the present study, a design acceleration time-history signal a_D was chosen from a typical set of mechanical shock test data. The a_D chosen had an envelope shape and peak amplitude representative of a mechanical shock pulse. The corresponding design shock response spectrum SRS_D , energy input spectrum EIS_D , envelope $E(t)$ and five temporal moments were determined from a_D . Figure (2-13) is a plot of the absolute value of a_D with $E(t)$ indicated on the plot. The peak value of the envelope $E(t)$ is 1.0, but was expanded by a factor of 47 in the plot to illustrate the fit with a_D . Figure (2-14) is a plot of SRS_D and EIS_D . The temporal moments of a_D are plotted on Figure (2-12). The five temporal moments and REA for the design acceleration a_D are,

- E_D (energy) $1.4053E6 \text{ in}^2/\text{sec}^2$
- τ_D (centroid) 0.0415 sec
- D_D (duration) 0.019 sec
- S_D (skewness) 0.0217 sec
- K_D (kurtosis) 0.0304 sec
- REA_D (root energy amplitude) $8,600 \text{ in}/\text{sec}^2$

For the present study, these design quantities were needed as a basis of comparison to evaluate the accuracy of synthesized accelerations a_S . These evaluations are the degree to which,

- SRS_S , EIS_S , and temporal moments of a_S match the corresponding quantities from a_D , and
- The accuracy of response of $MDOF$ models from a_S compared to the corresponding response from a_D .

3 New Approach to Synthesize SRS Compatible Acceleration

3.1 Overview

A new approach is described for the synthesis of an SRS compatible base acceleration beyond what has been proposed and implemented in the past. This includes the introduction of additional constraints beyond only SRS_D compatibility of the synthesized acceleration, a_S . These additional constraints for a_S are the design energy input spectrum (EIS_D) and five temporal moments determined from a_D . Given the objective to match multiple constraints, an optimization synthesis procedure was required. Two essential differences between how others have determined a_S and the proposed approach are specifically,

- a_S compatibility with EIS_D and a_D derived temporal moments in addition to SRS_D , and
- Quality of a_S evaluated based on the accuracy of $MDOF$ model response.

The significance of the additional constraints, or factors, was determined by regression analysis.

3.2 Traditional Synthesize Methods of SRS_D Compatible Base Acceleration

As described in Chapter 2, past authors have documented numerous methods to synthesize an SRS_D compatible base acceleration. Common synthesis methods include standard wave forms, typically comprised of a classical pulse or some variant of a summation of sinusoids. These methods include:

- Classical acceleration pulse (half sine, trapezoid, triangle, others),
- Damped sinusoids,
- Wavelets and
- Enveloped sinusoids with random phase angles.

Less commonly used methods include trained neural networks, inverse Fourier transforms, and maximum entropy.

Regardless of the method, authors have primarily addressed a single objective to synthesize a base acceleration, a_s , that returns a shock response spectrum, SRS_S , which matches the design shock response spectrum, SRS_D , within prescribed limits. For example, MIL-STD-810G, Method 516.6 (2008) prescribes a tolerance envelope of +3.0 dB/-1.5 dB around SRS_D which SRS_S is to meet. This single objective obviates the motivation to make use of aforementioned other significant information, specifically:

- Input energy per unit mass of a_s , characterized by an energy input spectrum EIS_S . The EIS of a general base acceleration $\ddot{u}_b(t)$ is determined from the right hand side of Eq. (2-33) and plotted on Figure (2-11).
- Five temporal moments described in Section 2.6 and indicated on figure (2-12).
- Transient shock shape envelope $E(t)$ indicated in Figure (2-13).

3.3 Synthesis of Base Acceleration a_s

The objective of the synthesis procedure is to determine a_s which is compatible with the corresponding design acceleration quantities of SRS_D , EIS_D , $E(t)$ and five temporal moments of a_D . To achieve this, the differences between synthesis based quantities SRS_S , EIS_S , and temporal moments of a_s , and the corresponding design quantities are minimized. The percent error factors for these synthesized quantities relative to the corresponding design quantities are given by Eqs. (3-1), (3-2) and (3-3), respectively. The envelope function $E(t)$ is imposed on the overall shape of a_s .

A synthesis optimization flow chart, Figure (3-1), illustrates this process. The approach is to minimize a merit function, M , that is a function of the percentage errors factors $SRS\%$, $EIS\%$, $E\%$, $\tau\%$, $D\%$, $S\%$ and $K\%$.

$$SRS\% = \frac{100}{N} \sum_{n=1}^N \left| \frac{SRS_S^n - SRS_D^n}{SRS_D^n} \right| \quad (3-1)$$

$$EIS\% = \frac{100}{N} \sum_{n=1}^N \left| \frac{EIS_S^n - EIS_D^n}{EIS_D^n} \right| \quad (3-2)$$

$$E\% = 100 \left(\frac{E_S - E_D}{E_D} \right) \quad (3-3)$$

$$\tau\% = 100 \left(\frac{\tau_S - \tau_D}{\tau_D} \right) \quad (3-4)$$

$$D\% = 100 \left(\frac{D_S - D_D}{D_D} \right) \quad (3-5)$$

$$S\% = 100 \left(\frac{S_S - S_D}{S_D} \right) \quad (3-6)$$

$$K\% = 100 \left(\frac{K_S - K_D}{K_D} \right) \quad (3-7)$$

The synthesis of a_s is given by Eq. (3-8). The synthesis method selected for the optimization of a_s was enveloped sinusoids with random phase angles. The envelope function $E(t)$ determines the temporal shape of a_s , provides control of the rise, plateau and decay of the synthesized wave form, rather than to rely on time delays and damping of individual sinusoids. Based on examination of mechanical shock acceleration data, a typical shock pulse has a rapid rise, a brief (if any) plateau, and a gradual decay. The correct choice of $E(t)$ assures this shape for a_s . It has proven to be effective in guiding the temporal profile of a_D , or the combined envelope in the case of a family of field data.

$$a_s(t) = E(t) \sum_{n=1}^N A_n \sin(\omega_n t + \phi_n). \quad (3-8)$$

The synthesis procedure is iterative as shown in Figure (3-1). The summation in Eq. (3-8) is over index n corresponding to N ω_n frequencies. The amplitude coefficients A_n are independently updated in each iteration to minimization the merit function M . To start the procedure, the following initial quantities are set.

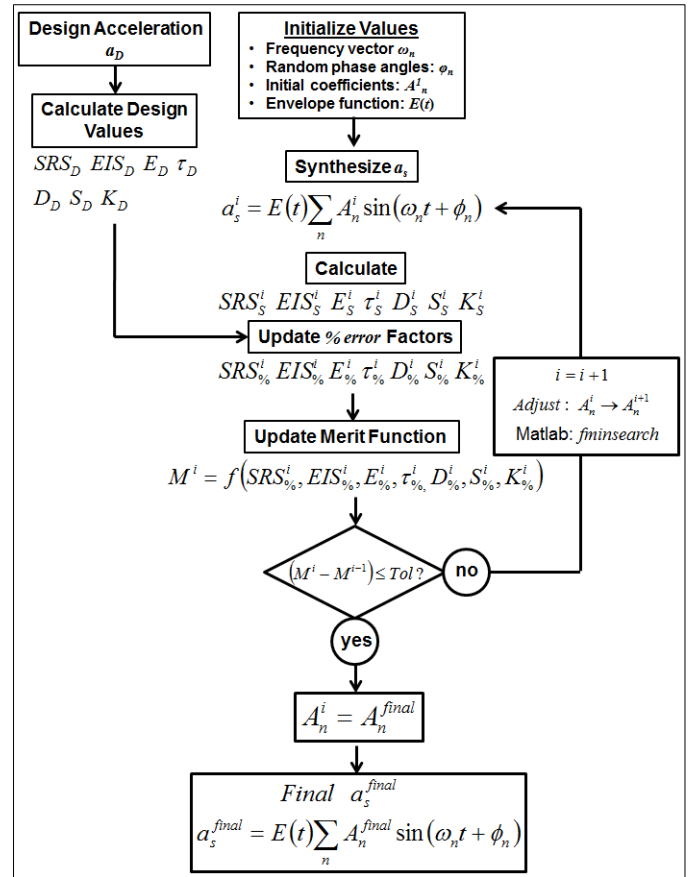


Figure (3-1). a_s Synthesis Optimization Process.

- Envelope function $E(t)$.
- Frequency vector ω_n to span the frequency bandwidth N .
- Vector of N random phase angles ϕ_n .
- Initial seed of N coefficients A_n , based on a percentage of SRS_D at each frequency.

$E(t)$, ω_n and ϕ_n are stationary during the optimization process. The optimization is executed over an iteration loop index i until the change to the merit function ΔM^i meets a predefined tolerance.

The synthesis process is started ($i=1$) by forming a_s using the initial values of A_n^1 . Initial values of A_n ($i=1$) were chosen to be 3% of SRS_D based on observations of prior results. Initial values of SRS_S^1 , EIS_S^1 , E_S^1 , τ_S^1 , D_S^1 , S_S^1 and K_S^1 are calculated from a_s^1 . As the process proceeds, the percentage errors given by Eq. (3-1) through (3-7) are calculated during each iteration i .

The merit function M^i , Eq. (3-9) is evaluated for each iteration i . A convergence criterion is given by Eq. (3-10).

$$M^i = f(SRS_S^i, EIS_S^i, E_S^i, \tau_S^i, D_S^i, S_S^i, K_S^i) \quad \text{and} \quad (3-9)$$

$$\Delta M^i = (M^i - M^{i-1}) \leq \text{Tol}. \quad (3-10)$$

This optimization process was executed with the Matlab optimization tool kit using the *fminsearch* routine⁶⁵. If ΔM^i does not meet the predefined tolerance of Eq. (3-6), the *fminsearch* optimization routine continues to adjust the set of A_n^i to further reduce M^i . When Eq. (3-10) is satisfied, a final set of amplitude coefficients, A_n^{final} , are used to compute the final synthesized acceleration a_s^{final} from

$$a_s^{\text{final}}(t) = E(t) \sum_{n=1}^N A_n^{\text{final}} \sin(\omega_n t + \phi_n) \quad (3-11)$$

3.4 Evaluate a_s from $MDOF$ Model Response

Regardless of how well the synthesized a_s meets the spectral and temporal factors of Eq. (3-1) through (3-7), there is no guarantee that when a_s is applied to a $MDOF$ model, the response of the model will agree with the corresponding response from the design acceleration, a_D . To evaluate a_s when applied to a physical model, the process of Figure (3-2) was developed. Both the design and

synthesized accelerations were applied to a general *MDOF* model. The model responses from a_s were compared to the corresponding responses from a_D .

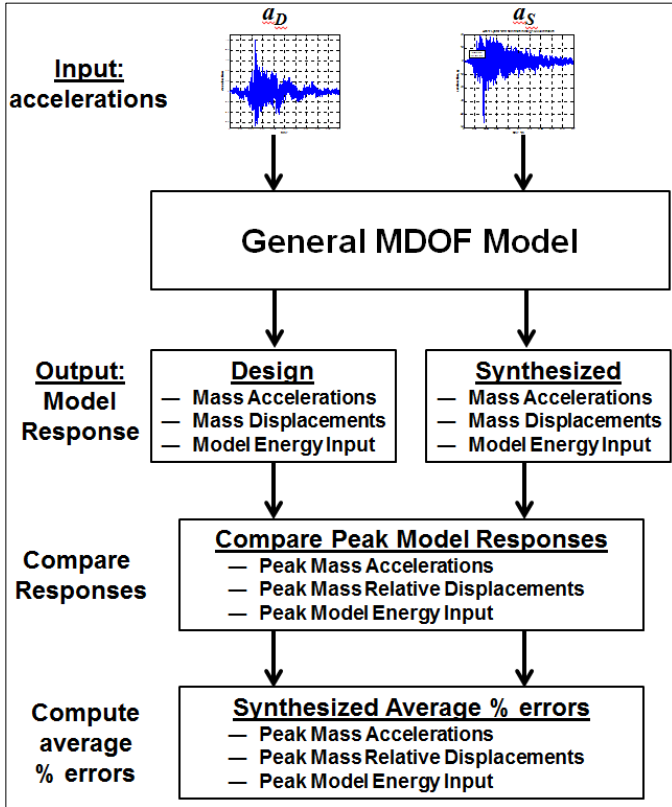


Figure (3-2). Process to Evaluate a_s Accuracy.

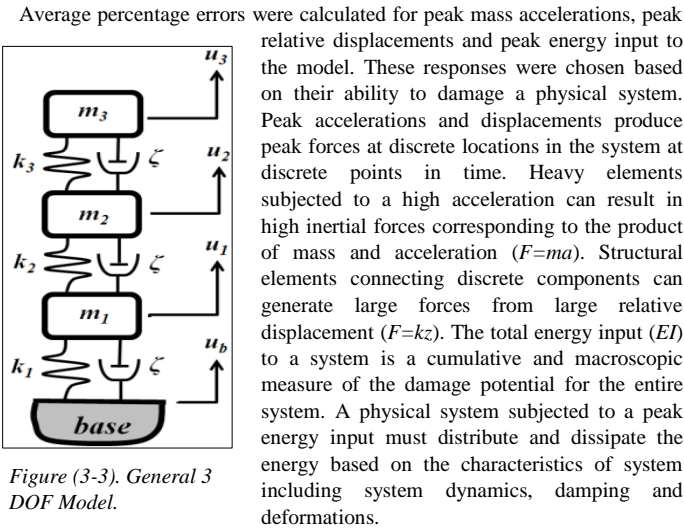


Figure (3-3). General 3 DOF Model.

Average percentage errors were calculated for peak mass accelerations, peak relative displacements and peak energy input to the model. These responses were chosen based on their ability to damage a physical system. Peak accelerations and displacements produce peak forces at discrete locations in the system at discrete points in time. Heavy elements subjected to a high acceleration can result in high inertial forces corresponding to the product of mass and acceleration ($F=ma$). Structural elements connecting discrete components can generate large forces from large relative displacement ($F=kz$). The total energy input (EI) to a system is a cumulative and macroscopic measure of the damage potential for the entire system. A physical system subjected to a peak energy input must distribute and dissipate the energy based on the characteristics of system including system dynamics, damping and deformations.

Three variants of the general *3DOF* model were developed based on three sets of spring force-displacement relationships given by,

- Linear: linear force-displacement relationship for all springs,
 - Nonlinear-Stiffening: nonlinear elastic springs where each spring rate increases when the displacement exceeds a predefined value and
 - Nonlinear-Softening: nonlinear elastic springs where each spring rate decreases when the displacement exceeds a predefined value.
- Details of the general *3DOF* model parameters are given in Appendix B.

As shown on Figure (3-2), average percentage errors were calculated based on the *3DOF* model response from a_s compare to the corresponding responses from a_D . These percent errors are,

- average percentage error of the peak mass accelerations,
- average percentage error of the peak relative displacements and
- percentage error of the *3DOF* model peak input energy.

These *3DOF* model response percentage errors are defined by Eq. (3-12), (3-13) and (3-14), respectively, where the superscript “s” is the *3DOF* response from the synthesized acceleration and superscript “D” is the *3DOF* response from the design acceleration. The *3DOF* model percentage errors are,

$$\ddot{u}_i\% \equiv \frac{100}{3} \sum_{i=1}^3 \frac{|\ddot{u}_i^s|_{\max} - |\ddot{u}_i^D|_{\max}}{|\ddot{u}_i^D|_{\max}}, \quad (3-12)$$

$$z_i\% \equiv \frac{100}{3} \sum_{i=1}^3 \frac{||z_i^s|_{\max} - |z_i^D|_{\max}|}{|z_i^D|_{\max}} \quad \text{and} \quad (3-13)$$

$$En\% \equiv 100 \left(\frac{En_{\max}^s - En_{\max}^D}{En_{\max}^D} \right). \quad (3-14)$$

The relative displacement for each mass m_i is defined by,

$$z_i \equiv u_i - u_b \quad (3-15)$$

3.5 Determine Significant Factors from Regression Analysis

The general merit function given by Eq. (3-9) includes seven percent error terms, or factors, to be minimized in the synthesis optimization process of Figure (3-1). The expectation is that minimization of these seven factors, given by Eq. (3-1) through (3-7), will improve system response accuracy when applied to a general *MDOF* system such as the *3DOF* model of Figure (3-3). However, it is unclear which factors are significant, or not significant, in reduction of the *MDOF* system errors given by Eq. (3-12) through (3-14). To quantify the significance of the seven factors, a regression analysis was completed for each of the three model responses. Fourteen unique acceleration-time histories were synthesized to execute the regression analysis. The assessment was completed for the three variants of the general *3DOF* model described in Appendix B (linear, nonlinear-stiffening, and nonlinear-softening). The regression analysis determined the significant factors for each model response, based on a predefined statistical significance threshold. A flow chat of this process is illustrated in Figure (3-4).

To execute the regression analysis, fourteen synthesized accelerations were applied to the *3DOF* model. Ten of the fourteen synthesized accelerations were developed by minimizing the merit function M in Eq. (3-16).

$$M = W_{SRS}SRS\% + W_{EIS}EIS\% + W_E E\% + W_{\tau} \tau\% + W_D D\% + W_S S\% + W_K K\% \quad (3-16)$$

Different combinations of the initial values of the weighting coefficients in Eq. (3-16) were chosen to synthesize 10 of 14 accelerations by the process described in Figure (3-1). As the matlab optimization process progressed (typically a 12-18 hours duration), real time changes were made to the weighting coefficients in (3-16) to best minimize the merit function M . The naming convention for these ten matlab synthesized accelerations contains the number of iterations.

In addition to the ten accelerations synthesized to minimize M , four synthesized accelerations plotted in Figure (2-7) were also included in the regression process. These four acceleration were synthesized to minimize $SRS\%$ only. The fourteen accelerations are plotted in Figure (3-5).

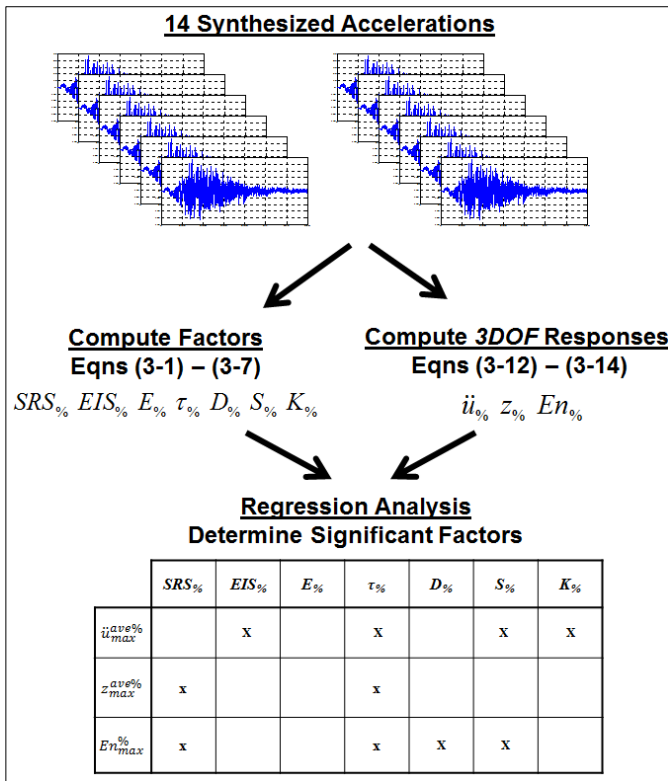


Figure (3-4). Regression Analysis Process.

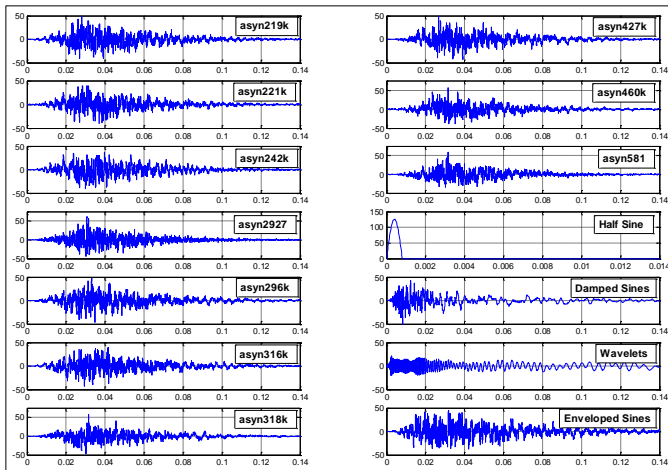


Figure (3-5). Fourteen Synthesized Accelerations.

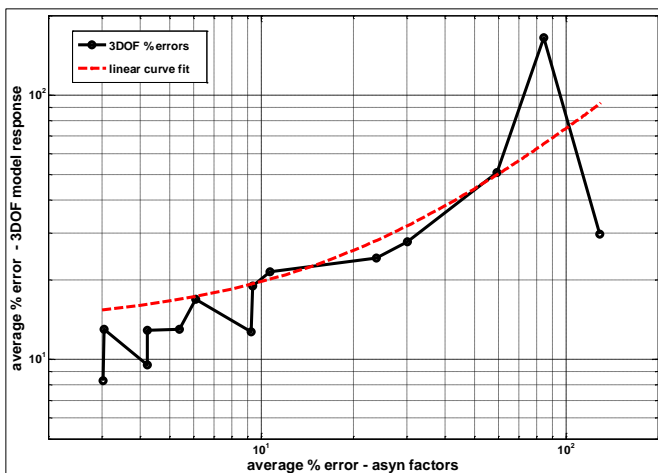


Figure (3-6). Correlation of 14 asyn Error Factors & 3DOF Model Response Errors.

The percent error factors, Eq. (3-1) through (3-7), for each of the 14 synthesized accelerations are tabulated in Table (3-1). The 3DOF model peak responses percent errors, corresponding to each of the synthesized accelerations, are tabulated in Table (3-2). The right hand columns of both tables are average percent errors for each row of all numerical columns. The right hand column of Table (3-1) represents the average of the seven percent error factors corresponding to each synthesized acceleration. The right hand column of Table (3-2) represents the average percent error of nine model response percent errors for the three variants of the general 3DOF model. Figure (3-6) is a plot of the average 3DOF model response percent error (right hand column of Table (3-2)) as a function of the synthesized accelerations factors percent error (right hand column of Table (3-1)). The solid black curve of Figure (3-6) is the plot of this relationship for all synthesized accelerations. The dashed red curve is a linear least squares fit to these 14 data points. It is evident that as the average percent error of the synthesized acceleration factors increase, in general the model response average percent error also increase. This general trend is not surprising. However, from this high level perspective the significance of each of the individual factors of Table (3-1) is not evident. Further, neither are the peak model responses errors (input energy, relative displacement and mass acceleration) that each individual factor may or may not influence. In order to address these questions, a set of nine individual regression analyses were executed; one for each of the nine model responses of Table (3-2).

Table (3-1). Regression Analysis Input Factors.

Synthesized Acceleration	$SRS_{\%}$	$EIS_{\%}$	$E_{\%}$	$\tau_{\%}$	$D_{\%}$	$S_{\%}$	$K_{\%}$	ave % error
asyn460k	4.88	4.65	-8.97	0.27	0.00	0.08	-2.28	3.02
asyn296k	4.18	7.38	-6.56	0.34	0.00	0.00	-2.93	3.05
asyn427k	4.46	5.63	10.30	1.17	2.54	-1.12	-4.33	4.22
asyn316k	6.24	6.22	-8.87	-0.97	3.70	3.60	0.00	4.23
asyn219k	5.99	13.74	-0.05	0.18	-2.49	-6.92	-8.33	5.39
asyn318k	9.31	8.54	15.12	1.03	0.66	-2.65	-5.30	6.09
asyn221k	8.07	9.96	14.33	-1.54	-9.96	10.14	10.88	9.27
asyn242k	14.01	25.58	0.00	0.03	-4.56	10.73	10.56	9.35
asyn581	12.93	8.95	-9.08	-3.31	13.07	13.63	13.81	10.6
asyn2927	47.19	67.2	-1.03	-5.06	16.80	14.28	15.46	23.86
Env Sines	4.88	95.9	41.2	4.32	28.17	20.17	16.43	30.16
Wavelets	6.97	34.90	27.78	39.58	139.67	81.48	84.59	59.28
Half Sine	83.30	77.0	32.09	99.03	99.24	100.03	99.41	84.30
Dmpd Sines	8.67	49.90	13.25	11.16	234.60	306.70	276.07	128.62

The significance of the seven factors in the merit function M was determined from regression analysis, based on the response of the general 3DOF model. The regression analysis was conducted with Minitab software⁴⁴. The factors, Eq. (3-1) through (3-7), were the inputs to the regression model and the 3DOF model responses, Eq. (3-12) through (3-14), were the outputs. The factors' percent errors for each synthesized acceleration are tabulated in Table (3-1). The corresponding model response percent errors are tabulated in Table (3-2).

The significance of the seven factors given by Eq. (3-1) through (3-7) was determined from regression analysis, based on the peak responses of the general 3DOF model. The factors, Table (3-1), were the inputs to the regression model and the 3DOF model responses, Table (3-2), were used to determine the regression model results. A regression analysis was performed for each individual 3DOF model response. For example the regression model to predict $En_{\%}$ for the linear 3DOF model response, determined the coefficients $C_1 - C_8$ in the following linear equation of the form,

$$En_{\%} = C_1 + C_2(SRS_{\%}) + C_3(EIS_{\%}) + C_4(E_{\%}) + C_5(\tau_{\%}) + C_6(D_{\%}) + C_7(S_{\%}) + C_8(K_{\%}) \quad (3-17)$$

The regression analysis solves a set of linear equations determined from the synthesized acceleration results of Tables (3-1) and (3-2). For the linear 3DOF model, a set of responses $En_{\%}$ corresponding to each synthesized acceleration is

tabulated in Table (3-2). The corresponding set of input factors are tabulated in Table (3-1). This result is a set of linear equations. Unknowns C1-C8 are determined by solving this system of linear equations. It is noted that terms could be added to Eq. (3-17) for the product of the factors, which can also be significant based on results of a prior study⁵. However, for the seven factors in Eq. (3-17), a total of 28 synthesized accelerations would be required to determine coefficients for all individual factors and all products of individual factors. For the current study, time permitted only 14 accelerations to be synthesized, which was not sufficient to include all product terms were in the regression model.

Table (3-2). General 3DOF Model Response Percent Errors.

Synthesized Acceleration	En%			z% lin			udd%			ave % error
	Lin	NLstiff	NLsoft	Lin	NLstiff	NLsoft	Lin	NLstiff	NLsoft	
asyn460k	0.77	8.10	-10.11	9.97	3.20	7.84	4.35	13.19	17.22	8.31
asyn296k	-0.10	16.23	17.44	13.77	7.16	11.77	25.19	7.88	17.44	13.00
asyn427k	-2.12	2.36	12.85	13.51	2.33	9.98	18.19	21.04	3.20	9.51
asyn316k	-8.93	18.88	15.62	22.82	2.53	19.86	11.38	2.10	13.91	12.89
asyn219k	-3.46	8.19	8.34	8.71	11.46	26.73	23.50	11.93	18.60	13.44
asyn318k	-2.23	18.04	41.20	14.26	7.66	32.45	14.79	10.71	10.47	16.87
asyn221k	-1.04	13.24	-2.84	17.23	11.39	18.53	16.73	20.59	12.96	12.73
asyn242k	-1.97	-32.11	-11.93	16.22	9.00	29.09	23.87	26.08	19.95	18.91
asyn581	-0.48	30.97	-2.53	18.63	3.75	25.14	42.17	25.26	43.74	21.41
asyn2927	-33.79	-36.09	-24.91	21.19	27.17	21.82	18.35	24.22	10.39	24.21
Env Sines	24.92	53.60	44.51	15.58	4.20	47.93	16.92	27.22	15.76	27.85
Wavelets	96.89	144.3	122.6	15.58	5.07	38.36	21.71	6.81	6.90	50.91
Half Sine	136.3	61.38	285.5	157.8	63.24	270.6	197.9	179.9	130.9	164.8
Dmpd Sines	44.80	84.97	70.91	15.63	1.87	14.50	8.95	17.69	8.84	29.80

Beyond determining the coefficients for a linear equation, the significance of each factor is determined by the regression model. The significance threshold for each factor was based on $\alpha \leq 0.1$, which corresponds to a 10% probability that the null hypothesis cannot be rejected in favor of the alternative hypothesis. The null hypothesis, H_0 , is that all $C_i = 0$ in Eq. (3-17), except C_1 . The alternative hypothesis, H_1 , is that at least one $C_i \neq 0$, not including C_1 . For example, the regression analysis determined the following significant factors and coefficients in Eq. (3-17) to be,

$$En_{\%} = 10.83 - 0.762(SRS_{\%}) - 2.915(\tau_{\%}) + 1.931(D_{\%}) - 4.31(S_{\%}) + 3.41(K_{\%}) \quad (3-18)$$

In this case of peak energy input % error model response, the significant factors based on meeting or exceeding $\alpha \leq 0.1$ criteria were $SRS_{\%}$, $\tau_{\%}$, $D_{\%}$, $S_{\%}$ and $K_{\%}$.

Tables (3-3) through (3-5) summarize the results of individual regression analyses corresponding to the linear, nonlinear-stiffening and nonlinear-softening variant of the general 3DOF model, respectively. Each row of these tables represents an individual regression analysis. Factors that met the $\alpha \leq 0.1$ criteria are indicated with a black "x" in the corresponding cell of each table. Those factors that met a more restrictive $\alpha \leq 0.05$ criteria are indicated with a red "x" in the corresponding cell. Each regression analysis included the entire set of fourteen synthesized accelerations plotted in Figure (3-5). These results indicate for all variants of the 3DOF model, the last four temporal moments (centroid, duration, skewness and kurtosis) represent significant factors vis-à-vis the accuracy of model response. The last column of Table (3-3) through (3-5) list adjusted R^2 values. R^2 is a percentage of how well the regression model such as Eq. (3-18) explains the variability in model response. For example, the $En_{\%}$ R^2 value in Table (3-3) indicates that Eq. (3-18) explains approximately 98.7% of the variation in the response for the peak energy input percent error for the linear 3DOF model.

The regression model equations corresponding to the significant factors indicated in Table (3-3) through (3-5) are given in Eq. (3-19) through (3-27) below.

Regression Model Equations for **Linear 3DOF Model**:

$$z_{\%} = 14.27 - 1.7010 \tau_{\%} + 0.8024 D_{\%} - 0.5473 S_{\%} \quad (3-19)$$

$$\ddot{u}_{\%} = 34.56 - 2.274 \tau_{\%} - 6.048 S_{\%} + 6.721 K_{\%} \quad (3-20)$$

$$En_{\%} = 10.83 - 0.762 SRS_{\%} - 2.915 \tau_{\%} + 1.931 D_{\%} - 4.31 S_{\%} + 3.41 K_{\%} \quad (3-21)$$

Regression Model Equations for **Nonlinear Stiffening 3DOF Model**:

$$z_{\%} = 2.17 + 0.5551 SRS_{\%} - 0.1339 \tau_{\%} \quad (3-22)$$

$$\ddot{u}_{\%} = 23.71 + 0.1547 EIS_{\%} - 1.903 \tau_{\%} - 4.056 S_{\%} + 4.534 K_{\%} \quad (3-23)$$

$$En_{\%} = 17.27 - 1.001 SRS_{\%} - 2.195 \tau_{\%} + 2.479 D_{\%} - 1.563 S_{\%} \quad (3-24)$$

Regression Model Equations for **Nonlinear Softening 3DOF Model**:

$$z_{\%} = 15.52 + 0.1798 EIS_{\%} - 2.886 \tau_{\%} + 1.641 D_{\%} - 1.183 S_{\%} \quad (3-25)$$

$$\ddot{u}_{\%} = 42.63 - 0.380 EIS_{\%} + 0.695 E_{\%} - 2.118 \tau_{\%} - 6.04 S_{\%} + 6.78 K_{\%} \quad (3-26)$$

$$En_{\%} = -22.1 - 3.661 \tau_{\%} + 4.773 D_{\%} + 6.06 S_{\%} - 10.30 K_{\%} \quad (3-27)$$

Appendix D contains additional information about the regression analysis for the three variant of the general 3DOF model.

Table (3-3). General 3DOF Model-Linear-Significant Factors.

3DOF Response	Significant Factors							R^2_{adj}
	SRS%	EIS%	E%	$\tau_{\%}$	D%	S%	K%	
$z_{\%}$				x	x	x		99.1%
$\ddot{u}_{\%}$				x		x	x	96.8%
$En_{\%}$	x			x	x	x	x	98.7%

Table (3-4). General 3DOF Model, Nonlinear Stiffening-Significant Factors.

3DOF Response	Significant Factors							R^2_{adj}
	SRS%	EIS%	E%	$\tau_{\%}$	D%	S%	K%	
$z_{\%}$	x			x				95.6%
$\ddot{u}_{\%}$		x		x		x	x	97.8%
$En_{\%}$	x			x	x	x		83.5%

Table (3-5). General 3DOF Model, Nonlinear Softening-Significant Factors.

3DOF Response	Significant Factors							R^2_{adj}
	SRS%	EIS%	E%	τ %	D%	S%	K%	
$z\%$		x		x	x	x		98.7%
$\dot{u}\%$		x	x	x			x	95.5%
En%				x	x	x	x	97.3%

3.6 Selection of a_5 for Comparison with Current Practices

By examination of Table (3-1) it is apparent that the first ten accelerations, synthesized to minimize the merit function of Eq. (3-16), had significantly lower percentage errors for all factors, defined by Eq. (3-1) through (3-7), compared to the last four acceleration synthesized to minimize $SRS\%$ only, Eq. (3-1).

The average percentage errors for all factors are 7.9% and 75.6%, respectively. Further, based on examination of Table (3-2), the 3DOF model response errors corresponding to the first ten synthesized accelerations were considerably lower than the average percent error from the last four accelerations.

The average 3DOF model percentage errors are 15.1% and 68.3%, respectively.

This general metric suggests that accelerations synthesized to minimize all errors given by Eq. (3-1) through (3-7) results in improved MDOF model response, compared to MDOF errors from accelerations synthesized to minimize $SRS\%$ only.

Figure (3-6) supports this premise. To further test this thesis, synthesized acceleration $asyn_{427k}$ was selected for another comparison with the four accelerations synthesized to minimize $SRS\%$ only.

$asyn_{427k}$ had the third lowest percentage errors for all factors in Table (3-1) and the second lowest 3DOF model response percent errors in Table (3-2).

Synthesized acceleration $asyn_{427k}$ was applied to a second 3DOF model based on the US Navy's medium weight shock machine (MWSM) and the responses were compared to corresponding responses from the common synthesis methods described in Section 2.3 of Chapter 2. The results of this comparison are described in Chapter 4.

Plots of $asyn_{427k}$ and the corresponding SRS and EIS are plotted on Figures (3-7) through (3-9), including the comparative plots for the design acceleration, a_D .

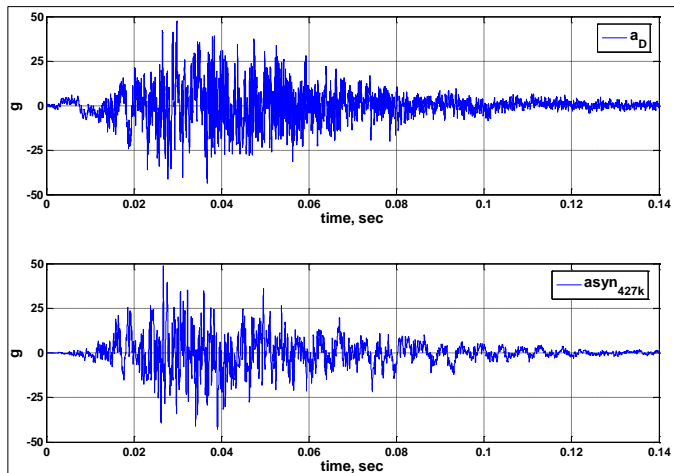


Figure (3-7). Design and Synthesized Accelerations, a_D and $asyn_{427k}$.

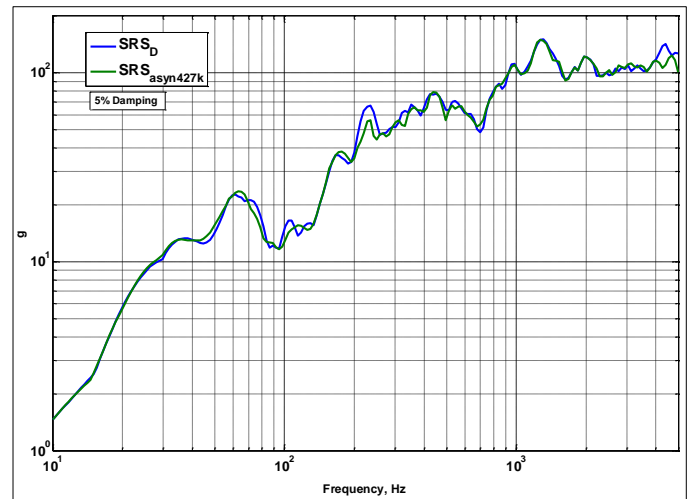


Figure (3-8). SRS_D and $SRS_{asyn427k}$.

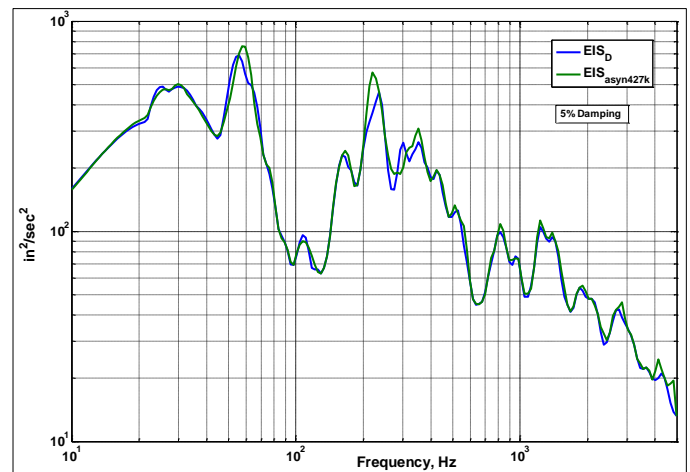



Figure (3-9). EIS_D and $EIS_{asyn427k}$.

Bibliography

- Alexander, J. E., "A Nonlinear DDAM Procedure," SAVIAC Proceedings of the 66th Shock and Vibration Symposium, Vol. 1, pp. 251-262. Biloxi, MS, 1995.
- Alexander, J. E., "Structural Analysis of a Nonlinear System Given a Shock Response Spectrum Input," SAVIAC Proceedings of the 69th Shock and Vibration Symposium, Unlimited Volume. Minneapolis, MN, 1998.
- Alexander, J. E., "Shock Response Spectrum-A Primer," Sound and Vibration, Vol. 43, No. 6, pp. 6-15, 2009.
- Alexander, J. E., "Application of Energy Methods in Mechanical Shock to Study Base Excited Nonlinear System Response," Conference Proceedings of the Society for Experimental Mechanics. Vol. 5, pp. 157-175, Rotating Machinery, Structural Health Monitoring, Shock and Vibration, 2011.
- Alexander, J. E., "A New Method to Synthesize a Shock Response Spectrum Compatible Base Acceleration to Improve Multi-Degree of Freedom system Response," (Doctoral dissertation), University of Minnesota, 2015.
- Barry Controls. (n.d.), SLM Mount Series, Retrieved August 15, 2015, from http://www.barrycontrols.com/userfiles/file/product_catalog/machinery/bcdi_prod_machinery_catalog.pdf
- Bathe, K., Gracowski, S., "On Nonlinear Dynamic Analysis Using Substructuring and Mode Superposition," Computers & Structures, Vol. 13, pp. 699-707, 1981.
- Biot, M., "Transient Oscillations in Elastic Systems," California Institute of Technology, 1932.
- Brake, M. R., "An Inverse Shock Response Spectrum," Mechanical Systems and Signal Processing, Vol. 25, pp. 2654-2672, 2011.

10. Bureau of Ships, "Shock Design of Shipboard Equipment, Dynamic Design-Analysis Method," Navy Department, Bureau of Ships, Washington D.C., 1961.
11. Chang, C. J., Mohraz, B., "Modal Analysis of Nonlinear Systems with Classical and Non-Classical Damping," *Computers & Structures*, Vol. 36, pp. 1067-1080, 1990.
12. Clements, E. W., "Shipboard Shock and Navy Devices for its Simulation, NRL Report 7396," Naval Research Laboratory, Washington, DC, 1972
13. Clough, H. L., Penzien, J., "In Dynamics of Structures," New York: McGraw Hill, 1975.
14. Dassault Systemes Simulia Corp, "Abaqus (Version 6.8)," Providence, RI, 2008.
15. Department of Defense, "MIL-STD-810G, Environmental Engineering Considerations and Laboratory Tests," Military Standard, 2008.
16. Department of the Navy, Naval Sea Systems Command, "Design Data Sheet 072-1, Shock Design Values," 1972.
17. Edwards, T. S., "Using Work and Energy to Characterize Mechanical Shock," Institute of Environmental Sciences and Technology, Annual Technical Meeting of the IEST, Conference Proceedings, ISBN: 978-1-60423-442-8, Vol 1, pp. 280-298, 2007.
18. Edwards, T. S., "Power Delivered to Mechanical Systems by Random Vibration," *Shock and Vibration*, Vol. 16, no. 3, pp. 261-271, 2009.
19. Gaberson, H. A., "Reasons for Presenting Shock Spectra with Velocity as the Ordinate," Proceedings of the 66th Shock and Vibration Symposium. SAVIAC, 1995.
20. Gasparini, D., Vanmarcke, E. H., "Simulated Earthquake Motions Compatible with Prescribed Response Spectra. Pub. No. R76-4," Evaluation of Seismic Safety of Buildings, Report No. 2, MIT, Department of Civil Engineering, 1976.
21. Ghaboussi, J., Lin, C. C., "New Method of Generating Spectrum Compatible Accelerograms Using Neural Networks," *Earthquake Engineering and Structural Dynamics*, Vol. 27, pp. 377-396, 1998.
22. Ghosh, A. K., "On the Generation of Ground Motion Accelerogram Compatible with a Specified Response Spectrum and a Fourier Amplitude Spectrum," *SMIRT 11 Transactions*, Vol. 11, pp. 7-12, 1991.
23. Gupta, I. D., Trifunac, M. D., "Defining Equivalent Stationary PSDF to Account for Nonstationarity of Earthquake Ground Motion," *Soil Dynamics and Earthquake Engineering*, Vol. 17, pp. 89-99, 1998.
24. Hartwig, T., "Evaluation of Transportation Vibration Associated with Relocation of Work in Process as Part of KCRIMS," Honeywell, Federal Manufacturing & Technology, Kansas City, MO, 2013.
25. Housner, G. W., "Characteristics of Strong Motion Earthquakes," *Bulletin of the Seismological Society of America*, Vol. 37, No. 1, pp. 19-31, 1947.
26. Housner, G. W., "Properties of Strong Ground Motion Earthquakes," *Bulletin of the Seismological Society of America*, Vol. 45, No. 3, pp. 197-218, 1955.
27. Housner, G. W., "Behavior of Structures During Earthquakes," *Journal of the Engineering Mechanics Division (ASCE)*, pp. 109-129, 1959.
28. Housner, G. W., Jennings, P. C., "Generation of Artificial Earthquakes," *Journal of the Engineering Mechanics Division (ASCE)*. Vol. 90, pp. 113-150, 1964.
29. Hudson, D. E., "Response Spectrum Techniques in Engineering Seismology," Proceedings of the World Conference on Earthquake Engineering, 1956.
30. Berkeley, C. A., "International Test and Evaluation Steering Committee, FR/GE/UK/US," International Test Operations Procedure (ITOP) 4-2-828, Ballistic Shock Testing, 2000.
31. Irvine, T., "Shock And Vibration Response Spectra Course Unit 29, Shock Response Spectrum Synthesis via Wavelets, 2015, June 24). Retrieved 2015, from http://www.vibrationdata.com/Course_Units/UNIT29.pdf.
32. Iwasa, T., Shi, Q., Saitoh, M., "Shock Response Spectrum Based on Maximum Total Energy of Single Degree of Freedom Model," AIAA 2008-1742, 49th Structural Dynamics and Materials Conference. Schaumburg, IL.: AIAA/ASME/ASCE/ASC Structures, 2008.
33. Iyengar, R. N., Iyengar, K. T., "Nonstationary Random Process Model for Warthquake Accelerograms," *Bulletin of the Seismological Society of America*, Vol. 59, No. 3, pp. 1163-1188, 1969, June.
34. Iyengar, R. N., Rao, P. N., "Generation of Spectrum Compatible Accelerograms," *Earthquake Engineering and Structural Dynamics*, Vol. 7, pp. 253-263, 1979.
35. Jennings, P. C., Housner, G. W., Tsai, N. C., "Simulated Earthquake Motions," California Institute of Technology, Earthquake Engineering Research Laboratory, Pasadena, 1968.
36. Kost, G., Tellkamp, T., Gantayat, A., Weber, F., "Automated Generation of Spectrum-Compatible Artificial Time Histories," *Nuclear Engineering and Design*, Vol. 45, pp. 243-249, 1978.
37. Kukreti, A. R., Issa, H. I., "Dynamic Analysis of Nonlinear Structures by Pseudo-Normal Mode Superposition Method," *Computers & Structures*, Vol. 19, pp. 653-663, 1984.
38. Lee, S. C., Han, S. W., "Neural Network Based Models for Generating Artificial Earthquakes and Response Spectra," *Computers and Structures*, Vol. 80, pp. 1627-1638, 2010.
39. Levy, S., Wilkinson, J. P., "Generation of Artificial Time-Hiostories, Rich in All Frequencies, From Given Response Spectra," *Nuclear Engineering and Design*, Vol. 38, pp. 241-251, 1976.
40. Lin, Y., Sun, T., "Mode Superposition Analysis of Viscously Damped Nonlinear Structural Systems Using an Incremental Algorithm," *Journal of Vibration and Acoustics*, Transactions of the ASME, Vol. 115, pp. 397-402, 1993.
41. Manfredi, G., "Evaluation of Seismic Energy Demand," *Earthquake Engineering and Structural Dynamics*, Vol. 30, pp. 485-499, 2001.
42. MIL-STD-810G, Method 516.6, Shock, Department of Defense, Test Method Standard-Environmental Engineering Considerations and Labortaory Tests, 2008.
43. Ministry of Defense. Environmental Handbood for Defence Materiel, Part 3, Environmental Test Methods, DEF STAN 00-35 Part 3 Issue 4. MOD, 2006.
44. Minitab, Inc. Minitab (version 16). State College, PA, 2014, April.
45. NASA. Pyroshock Test Criteria, NASA Technical Standard, NASA-STD-7003, 1999.
46. NASA. Dynamic Environmental Criteria, NASA-HDBK-7005. NASA Technical Handbook, 2001.
47. Navy, U. S., "MIL-S-901D", 1989.
48. Nelson, D. B., "Parameter Specification for Shaker Shock Waveform Synthesis-Damped Sines and Wavelets," 60th Shock and Vibration Symposium, Vol. 3, pp. 151-193. Portsmouth: Shock and Vibration Information Analysis Center (SAVIAC), 1989.
49. Newmark, N. M., Blume, J. A., Kapur, K. K., "Design Response Spectra for Nuclear Power Plants," American Society of Civil Engineers (ASCE) Structural Engineering Meeting, pp. 287-303, San Francisco: ASCE, 1973.
50. O'Hara, G. J., Belsheim, R. O., "Interim Design Values for Shock Design of Shipboard Equipment, NRL Memorandum Report 1396," U. S. Naval Research Laboratory, Feb, 1963.
51. Ordaz, M., Huerta, B., Reinoso, E., "Exact Computation of Input-Energy Spectra from Fourier Amplitude Spectra," *Earthquake Engineering and Structural Dynamics*, Vol. 32, pp. 597-605, 2003.
52. Preumont, A. (1980). A Method for the Generation of Artificial Earthquake Accelerograms. *Nuclear Engineering and Design*, 59, 357-368.
53. Preumont, A., "The Generation of Spectrum Compatible Accelerograms for the Desigh of Nuclear Power Plants," *Earthquake Engineering and Structural Dynamics*, Vol. 12, pp. 481-497, 1984.
54. Rizzo, P. C., Shaw, D. E., Jarecki, S. J., "Development of Real/Synthesized Time Histories to Match Smooth Design Spectra," Berlin: International Conference on Structural Mechanics in Reactor Technology, 1973.
55. Saragoni, G. R., Hart, G. C., "Simulation of Artificial Earthquakes," *Earthquake Engineering and Structural Dynamics*, Vol. 2, pp. 249-267, 1974.
56. Scanlan, R. H., Sachs, K., "Earthquake Time Histories and Response Spectra," *Journal of the Engineering Mechanics Division*, Vol. 100, pp. 635-655, American Society of Civil Engineering, 1974.
57. Shah, V. N., Bohm, G. J., Nahavandi, A. N., "Modal Superposition Method for Computationally Economical Nonlinear Structural analysis," Montreal: Transactions of the ASME, Vol. 101, pp. 134-141, 1979.

58. Shinozuka, M., "Digital Simulation of Ground Accelerations," 5th World Conference of Earthquake Engineering, pp. 2829-2838, Rome, 1973.
59. Smallwood, D. O., "Shock Testing on Shakers by Using Digital Control," Institute of Environmental Sciences. Mount Prospect: Institute of Environmental Sciences, 1986.
60. Smallwood, D. O., "Characterizing Transient Vibrations Using Band Limited Moments," Proceedings of the 60th Shock and Vibration Symposium, Vol. 3, pp. 93-111, Virginia Beach, VA, 1989.
61. Smallwood, D. O., "Variance of Temporal Moment Estimates of a Squared Time History," Proceedings of the 63rd Shock and Vibration Symposium, Vol. 1, pp. 389-399, Las Cruces, NM, 1992.
62. Smallwood, D. O., "Characterization and Simulation of Transient Vibrations Using Band Limited Temporal Moments," Shock and Vibration, Vol. 1, No. 6, 507-527, 1994.
63. Smallwood, D. O., Nord, A. R., "Matching Shock Spectra with Sums of Decaying Sinusoids Compensated for Shaker Velocity and Displacement Limitations," Shock and Vibration Bulletin, Vol. 44, pp. 43-56, 1974.
64. Soize, C., "Information Theory for Generation of Accelerograms Associated with Shock Response Spectra," Computer-Aided Civil and Infrastructure Engineering, Vol. 25, pp. 334-347, 2010.
65. The Mathworks, Inc. Matlab (Version R2014a). Natick, MA, 2014, August.
66. Trifunac, M. D., "Early History of the Response Spectrum Method. Soil Dynamics and Earthquake Engineering, Vol. 28, pp. 676-685, 2008.
67. U. S. Nuclear Regulatory Commission, Office of Nuclear Regulatory Research, Regulatory Guide 1.60, Revision 2. NRC, 2014.
68. Uang, C. M., Berto, V. V., "Evaluation of Seismic Energy in Structures," Earthquake Engineering and Structural Dynamics, Vol. 19, pp. 77-90, 1990.
69. Villaverde, R., "Modal Superposition Method for Seismic Design of Non-Linear Multistorey Structures," Earthquake Engineering and Structural Dynamics, Vol. 16, pp. 691-704, 1988.
70. Villaverde, R., "Simplified Response-Spectrum Seismic Analysis of Nonlinear Structures," Journal of Engineering Mechanics, pp. 282-285, 1996.
71. Zahrah, T. F., Hall, W. J., "Earthquake Energy Absorption in SDOF Structures," Journal of Structural Engineering, Vol. 110, pp. 1757-1772, 1984.
72. Zhang, C., Chen, C., Li, M., "Earthquake Accelerogram Simulation with Statistical Law of Evolutionary Power Spectrum," ACTA Seismologica Sinica, Vol. 20, pp. 435-446, 2007. 

The author can be reached at: alexanje53@aol.com